Curvature-induced motion of a thin Bingham layer in airways bifurcations

Cyril Karamaoun, Haribalan Kumar, Médéric Argentina, Didier Clamond, Benjamin Mauroy

.

Curvature-induced motion of a thin Bingham layer in airways bifurcations

Cyril Karamaoun,[1] Haribalan Kumar,[2] Médéric Argentina,[3] Didier Clamond,[1] and Benjamin Mauroy[4,*]

[1] *Université Côte d'Azur, LJAD, VADER Center, Nice, France*
[2] *Auckland Bioengineering Institute, Auckland, New-Zealand*
[3] *Université Côte d'Azur, Institut de Physique de Nice, VADER Center, Nice, France*
[4] *Université Côte d'Azur, CNRS, LJAD, VADER Center, Nice, France*

(Dated: December 22, 2021)

On the bronchi walls, the bronchial mucus forms a thin layer that protects the lung by capturing inhaled pollutants. Due to the curvature of its interface with air, the layer is submitted to curvature effects that interact with its rheology. Based on lubrication theory and 3D simulations, we show that these effects might move overthick mucus layers in the airway bifurcations. This movement could disrupt the mucociliary clearance and break the layer thickness homogeneity.

The lung constitutes a large interface between the atmosphere and the body, with a surface area of about 75–100 m^2 [1, 2]. Thus, it is a potential entry point into the body for external contaminants – dust particles, chemicals, bacteria, viruses – that can be inhaled during ventilation. In order to deal with these contaminants, protection mechanisms are present. One of these mechanisms is based on a layer of bronchial mucus that lines the bronchi walls [3]. The mucus acts as a trap for inhaled contaminants and is displaced upwards along the bronchi, up to the larynx, where it is either expelled or swallowed. Two main phenomena are responsible for the mucus displacement [4]. First, the bronchial epithelium includes ciliated cells and, by beating, the cilia push the mucus toward the trachea. This phenomenon is called the mucociliary clearance [4, 5]. Second, during cough [6, 7] or even high ventilation rates [8], exhaled airflows are high enough to interact with the mucus, and to drag it upward the bronchial tree. The efficiency of the protection by the mucus is dependent on the proper functioning of these two phenomena. Pathologies such as asthma, chronic obstructive pulmonary disease (COPD) or cystic fibrosis can impair the mucociliary clearance, leading to major respiratory symptoms and to infections [9–11]. The mucociliary clearance and the air–mucus interaction have been explored thoroughly in the literature [7, 8, 12–18].

The role of the surface tension on the air–mucus interface is however often neglected [19, 20]. The surface tension induces a jump of pressure –the Laplace pressure– across a curved interface: $\Delta p_L = 2\gamma\kappa$ with γ the coefficient of surface tension and κ the mean curvature of the interface. We can evaluate the distribution of this pressure in a common model of the bronchial tree [1, 21–25]. The lung is considered as a bifurcating tree whose branches are perfect cylinders that decrease in size at each bifurcation with an homothetic factor $h = (1/2)^{1/3} \simeq 0.79$. In such a model, the airways are indexed by their generation i that represents the number of bifurcations from the airway in focus to the root of the tree that mimics the trachea. The radii of the airways in the generation i is $r_i = h^i\, r_0$, with r_0 the radius of the root of the tree. If we consider that the air–mucus interface has a curvature similar to that of the airways walls, in an airway of generation i, the Laplace pressure is $p_{L,i} = -\gamma/r_i$. This pressure decreases with the generation index, i.e. the curvature effects, tend to push the layer toward the deeper parts of the tree. The resulting stress in a layer with thickness τ is $\sigma_i \simeq \gamma \frac{h-1}{r_i^2}\frac{\tau}{2}$, see Appendix A. It tends to increase along the generations of the tree, hence affecting more strongly the layers in the small bifurcations. However, a more local and detailed analysis is needed to evaluate if it can move the mucus or not, including detailed shapes of the bifurcations and more realistic mucus hydrodynamics and rheology [26].

Actually, mucus is a complex viscoelastic fluid, potentially thixotropic [26]. Its rheological properties depend on the person, the localization of the mucus in the bronchial tree and the environment – air humidity, temperature, etc. Mechanical constraints also influence the mucus behavior, and one of its core properties is to present a yield stress σ_y under which it behaves like a pseudo–solid material [8, 13, 14, 17, 26]. This characteristic induces that the inner shear stresses in the fluid have to overcome σ_y in order for the mucus to behave as a fluid of viscosity μ. The typical healthy thickness τ of the mucus layer is of the order of magnitude of 10 μm [27]. To understand under which conditions the surface tension effects could be large enough to overcome the mucus yield stress, we modelled the mucus as a Bingham fluid. This approach has already brought rich insights in the behavior of the bronchial mucus layer [13, 14]. Furthermore, it allows for capturing fundamental non–linear dynamics of the layer that could not be represented well with a pure Newtonian fluid approach.

The Reynolds number associated to the mucus in the airways is low and the fluid mechanics is well approximated by the Stokes equations. Then, denoting $\mathbf{u}$ the fluid velocity and p its pressure, the momentum and mass

* benjamin.mauroy@unice.fr

Quantity	Value (ref value)	Notation	Ref
Lungs' geometrical data			
trachea radius	0.01 m	r_0	[1]
reduction factor	$(1/2)^{\frac{1}{3}} \sim 0.79$	h	[1, 22, 23]
Mucus properties			
surface tension	0.03 Pa.m	γ	[28]
mucus layer thickness (healthy)	5 - 30 μm (10)	τ	[15]
mucus viscosity	10^{-3} - 10 Pa.s (1)	μ	[26]
mucus yield stress	10^{-2} - 10 Pa (0.1)	σ_y	[26]
cilia induced mucus velocity	10 - 500 μm.s^{-1} (50)	v_{cilia}	[20, 27, 29]

TABLE I. Data range of the parameters of our model and their default values used in this paper, shown between parentheses.

conservation equations are

$$\begin{cases} \rho\frac{\partial \mathbf{u}}{\partial t} - \nabla.\Sigma = \nabla p & \text{in the layer} \\ \nabla.\mathbf{u} = 0 & \text{in the layer} \\ \Sigma.\mathbf{n}_{\mathcal{L}} - p\,\mathbf{n}_{\mathcal{L}} = p_L\,\mathbf{n}_{\mathcal{L}} & \text{at the air–fluid interface } \mathcal{L} \\ \mathbf{u} = 0 & \text{on the airway wall } W \\ \frac{\partial \mathbf{X}_{\mathcal{L}}}{\partial t} = (\mathbf{u}(\mathbf{X}_{\mathcal{L}}).\mathbf{n}_{\mathcal{L}})\,\mathbf{n}_{\mathcal{L}} & \text{at the interface } \mathcal{L}, \text{ for } \mathbf{X}_{\mathcal{L}} \in \mathcal{L} \\ p_L = -2\gamma\kappa(x,y,z,t) & \text{at the interface } \mathcal{L} \end{cases} \tag{1}$$

The vector $\mathbf{n}_{\mathcal{L}}$ is the normal to the air–Bingham fluid interface $\mathcal{L}$ and the quantity κ is the mean curvature of this interface. The normals are oriented towards the air medium. The characteristic thickness of the layer along these normals is denoted τ. The tensor Σ is the stress tensor in the fluid. We assume a quasi-static response of the Laplace pressure to curvature changes. The air–Bingham fluid interface $\mathcal{L}$ is a free surface and a geometrical point $X_{\mathcal{L}}$ of its surface is moving with the normal component of the Bingham layer velocity, $(\mathbf{u}(\mathbf{X}_I).\mathbf{n}_{\mathcal{L}})\,\mathbf{n}_{\mathcal{L}}$. Finally, we assume a non slip boundary condition at the wall in order to capture the sole effect of the surface tension on the layer. We will superimpose the role of the mucociliary clearance as a second step.

The Bingham fluid constitutive equations are

$$\begin{cases} \Sigma = \left(\mu + \frac{\sigma_y}{\dot\gamma}\right)\dot\Gamma & \text{for } \sigma > \sigma_y \\ \dot\Gamma = 0 & \text{for } \sigma \le \sigma_y \end{cases}$$

with $\dot\Gamma = \frac{1}{2}\left(\nabla u + {}^t\nabla u\right)$ the rate of strain tensor and with $\sigma = \sqrt{\frac{1}{2}\Sigma{:}\Sigma}$ and $\dot\gamma = \sqrt{\frac{1}{2}\dot\Gamma{:}\dot\Gamma}$ the second invariants of, respectively, the stress tensor and the rate of strain tensor.

The layer thickness is, in general, small relatively to the curvature radius of the bronchi wall. Hence, planar lubrication theory [30, 31] applies to the previous system of equations. The full theoretical details are given in Appendix B. Our results show that the inner stresses in the Bingham fluid layer are mainly in the plane tangent to the airways walls. Moreover, they aligned with the air–Bingham fluid interface curvature gradient $\nabla_\xi\,\kappa$ with respect to the local coordinates system ξ. Our computations uncover a Bingham number associated to our system, $B = \frac{\sigma_y r^2}{2\gamma\tau}$, with r the characteristic radius of curvature of the interface, typically the radius of the airway considered. Our analysis brings a condition for the Bingham fluid layer to be liquid, $\nabla_{\tilde\xi}\,\tilde\kappa > B$, where $\nabla_{\tilde\xi}\,\tilde\kappa = r^2 \times \nabla_\xi\,\kappa$ is the normalised curvature gradient of the air–Bingham fluid interface with respect to the normalised local coordinates $\tilde\xi = \xi/r$.

As in [13, 14], a layer of liquid Bingham fluid spans from the airway wall over a proportion $e = \max\left(0, 1 - \frac{B}{\|\nabla_{\tilde\xi}\,\tilde\kappa\|}\right)$ of the thickness of the layer. Above this liquid layer, the Bingham fluid remains solid. When moving, the liquid layer drags the solid part of the layer as in [13, 14]. Because the surface tension tends to homogeneize the layer thickness, we assume now that the layer is of constant thickness τ and has the same curvature as the wall of the airways. Notice that this analysis assumes the airways to be perfectly smooth. Moreover, we do not account for large fluid accumulations, clots or plugs whose physics is not only affected by surface tension, but also by the air flow, as suggested in [13, 14, 17, 32]. Under these conditions and for an airway in the generation i, we determined the dominant velocity field $\mathbf{v_{st,i}}$ averaged over the thickness of the layer, see Appendix B 11,

$$\begin{aligned} \mathbf{v_{st,i}} = &\ -f(e_i)\ \frac{\gamma\tau^2}{\mu}\ r_i^2\ \nabla_{\tilde\xi}\,\tilde\kappa \\ \text{with } e_i = \max&\left(0, 1 - \frac{B_i}{\|\nabla_{\tilde\xi}\,\tilde\kappa\|}\right) \text{ and } f(e) = e^2\left(1 - \frac{e}{3}\right) \end{aligned} \tag{2}$$

The vector $-\frac{\gamma\tau^2}{\mu} r_i^2 \nabla_{\tilde\xi}\,\tilde\kappa$ is the typical velocity induced by curvature gradients of a thin layer of a Newtonian fluid on a non flat surface. The non Newtonian dynamics is fully driven by the dimensionless quantity $f(e_i)$. We denote $\mathbf{v_{cilia,i}}$ the velocity field induced by the mucociliary clearance. Then, the total velocity field in the generation i is $\mathbf{v_{m,i}} = \mathbf{v_{cilia,i}} + \mathbf{v_{st,i}}$

If we assume that a bifurcation of generation i is an homothetic transformation with the ratio h^i of the bifurcation of the first generation, we can compute a scaling law on the curvature gradients, $\nabla_{\xi^i}\,\kappa_i = h^{-2i}\ r_0^2\ \nabla_{\tilde\xi}\tilde\kappa$. The wall curvature field $\tilde\kappa$ is then estimated in an idealized 3D tree geometry, as depicted in Fig. 1A. This assumption leads to a scaling-law for the Bingham fluid velocity:

$$\mathbf{v_{st,i}} = \left(\frac{1}{h^2}\right)^i f(e_i)\ {r_0}^2\ \frac{\gamma\tau^2}{\mu}\nabla_{\tilde\xi}\tilde\kappa, \tag{3}$$

The curvature and gradients of curvature are computed numerically on a triangular mesh of a 3D geometry surface of an airway tree, see Fig. 1A and Appendix D. Then, the Bingham fluid velocities on this surface are computed based on the theoretical formula (2). Finally, we modeled the mucociliary clearance in the 3D airway

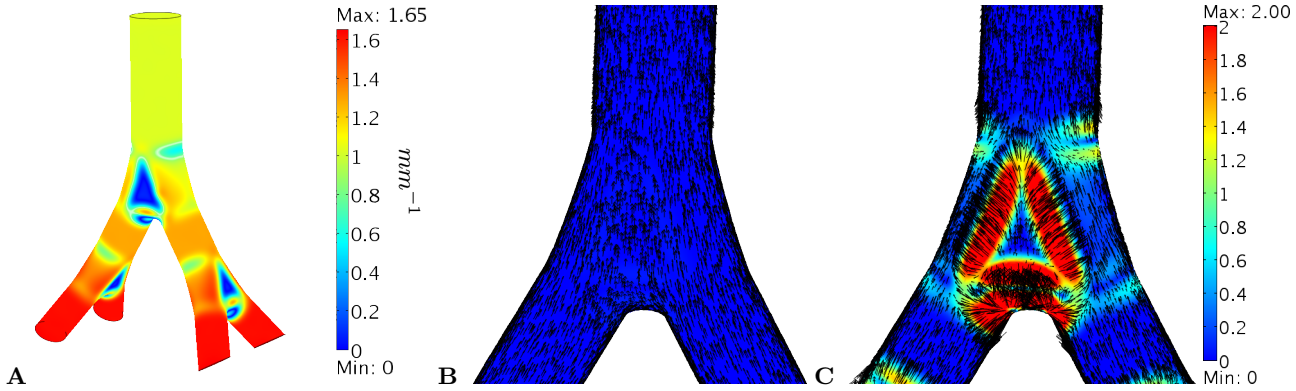

FIG. 1. **A**: The reference 3D geometry used with the lubrication theory. The geometry is rescaled in order to cover the whole scales of the bifurcations in the bronchial tree. The branches size decreases with a ratio $h = (1/2)^{\frac{1}{3}}$ at the bifurcations. The branching angle is 60° and the angle between the two successive branching planes is 90° in accordance with the mean observed values [23]. The colors represent twice the non signed mean curvature field $|\kappa_0|$ (m^{-1}) in the case of a root branch radius of 1 mm. **B** ($\tau = 10$ μm), **C** ($\tau = 75$ μm): Bingham fluid velocity fields $\mathbf{v_{m,i}}$ (arrows) and ratio α between the amplitudes of the velocity induced by the surface tension effects and of the velocity induced by the idealised mucociliary clearance, i.e. $\alpha = \|\mathbf{v_{st,i}}\|/\|\mathbf{v_{cilia}}\|$ (colors). In this case, the mother branch has a radius of 1 mm and the daughter branches a radius of $(1/2)^{1/3} \simeq 0.79$ mm. At physiological thickness (B), only the idealised mucociliary clearance is driving the motion of the mucus. For non healthy thickness (C), The idealised mucociliary clearance is altered by the surface tension effects.

tree to be tangential to airways walls. The clearance is directed toward the larger airways [20] and has an amplitude of 50 μm [27], see Appendix E. Typical outputs are presented in Fig. 1. For thicknesses corresponding to healthy mucus layers – about 10 μm [15] – the curvature gradients are too weak to affect the idealised mucociliary clearance, see Fig. 1B. However, if the thickness increases, the velocity field becomes less and less dominated by the mucocilliary clearance. Eventually, the mucociliary clearance loses progressively its organised patterns, up to a point where it breaks into local velocity fields driven only by local curvature, see Fig. 1C. Interestingly, the increased thickness of the mucus layer in pathological conditions has been associated with a disturbance of the mucociliary clearance [9–11]. These results highlight the importance of the mechanisms of control of the mucus thickness, in particular in the bifurcations [27].

The perturbation of the mucociliary clearance might lead to inhomogeneous distributions of the layer thicknesses, with regions where it accumulates and regions where it is depleted. Our model shows that the layer thickness and its localization in the bifurcation define where local mucus accumulation or depletion could occur, see Fig. 1C. A local accumulation might increase the risk of bronchial obstruction. A local depletion reduces the protection of the epithelium, making it more susceptible to external contaminants. Furthermore, our model suggests that local accumulation of mucus should develop first at the outlet of the mother bronchus, and at the inlet of the daughter bronchi. To the contrary, the carina of the bifurcation, i.e. the meeting point of the two daughter bronchi, presents a relatively low curvature, as seen in Fig. 1A. This makes this region more susceptible to mucus depletion and, consequently, to aggression from the deposition of external contaminants. Moreover, inhaled particules are more likely to deposit themselves at the carina [33, 34]. Thus, mucus overproduction might counterintuitively increase the risk of epithelial damage near the carina [33].

To get a global picture of the phenomenon, we quantified directly the opposite influence of the curvature gradients on the mucociliary clearance in a bifurcation. We projected the velocity field induced by the surface tension on the local direction of the idealized mucociliary clearance, and averaged this velocity field over the layer thickness and over the bifurcation, as described in Appendix C. Various mucus thicknesses were tested; the results are shown in Fig. 2A. Altogether, even for layer thicknesses corresponding to a healthy state, the surface tension gradients overcome the Bingham fluid yield stress starting from the 13^{th} generation. This implies that, from this generation to deeper ones, the fluid would adopt a liquid behavior and could be displaced. However, as shown in Fig. 2, it does not affect notably the mucociliary clearance in these generations, as the magnitude of the resulting velocities is small.

The velocity opposing the mucociliary clearance is strongly affected by the non Newtonian behavior of the Bingham fluid, which is fully driven by the Bingham number $B_i = \frac{\sigma_y r_i^2}{2\gamma\tau}$, as shown in Fig. 2B. Indeed, once normalized by the velocity that a Newtonian fluid would have in the same configuration, the velocities opposing the mucociliary clearance depend only on the Bingham number. At Bingham numbers smaller than about 0.1, the Bingham fluid is liquid everywhere. Nevertheless, the overcoming of the yield stress makes the fluid move at about 20% of the velocity that a Newtonian fluid would have in the same conditions. The velocities drop drasti-

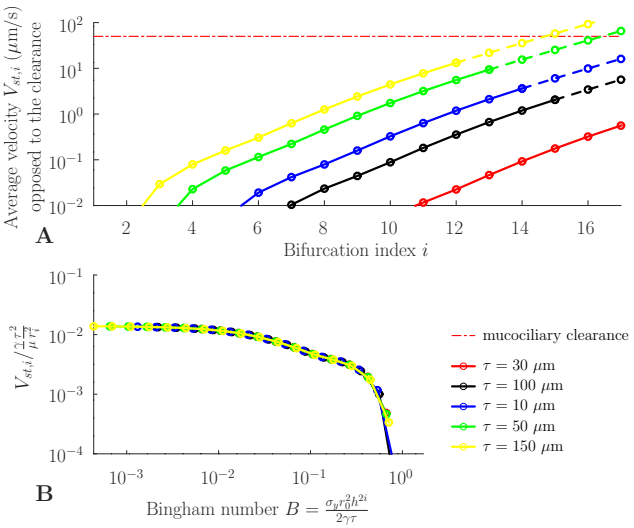

FIG. 2. **A:** Surface tension induced velocity of the Bingham layer in the direction of the idealised mucociliary clearance, averaged over the whole bifurcation and over the layer thickness. The parameters used are $\sigma_y = 0.1\ Pa$, $\mu = 1\ Pa.s$ and a mucociliary clearance amplitude of 50 $\mu m.s^{-1}$. In a thick layer, the surface tension is able to notably oppose the mucociliary clearance. The dashed parts of the curves correspond to the regions where the model hypothesis $\tau/r_i << 1$ loses its validity (i.e. $\tau/r_i > 10\%$). **B:** Velocity opposing the mucociliary clearance normalised by the velocity of a Newtonian fluid in the same configuration. Once normalized, the velocity depends only on the Bingham number. The velocity drops for Bingham numbers larger than about 0.5, indicating that the fluid inner stresses are not large enough to fully liquify the Bingham fluid.

cally when the Bingham number is larger than about 0.5. In this case, the Bingham fluid is no more fully liquid and eventually becomes fully solid.

In the absence of mucociliary clearance, the Bingham fluid would tend to be displaced backwards by the curvature gradients, toward the deeper generations. This displacement would stop eventually, as the magnitude of these gradients vanishes in the cylindrical airways. As a consequence, local accumulations of fluid could occur in these generations. Hence, our analysis suggests that the mucociliary clearance might also play a role to compensate the surface tension effects on the mucus distribution in the bifurcations, to avoid the disruption of the layer homogeneity. Moreover, the surface tension gradients trigger the displacement of the layer with a velocity vector that is primarily placed in the plane of the layer. Hence, this suggests that they contribute to maintain the flat geometry of the layer, and to stabilize its thickness inside the bifurcation. However, when the layer is too thick, the surface tension might become too strong for the mucociliary clearance to counteract its effects.

Our results uncover for the first time the rich behavior induced by the surface tension at an air–Bingham fluid interface in airway bifurcations. They put a new light on the possible consequence of pathological thickening of the mucus layer in the bronchi, which might counteract, and potentially disrupt the mucociliary clearance. However, the application of our results to the bronchial mucus layer has to account for the model hypotheses. The influence of curvature gradients on the bronchial mucus layer remains an intricate phenomenon.

First, the rheology of real mucus is complex and not well understood. Moreover, mucus properties are known to present a high level of variability [26], depending on the individual and the environment. Hence, studying this problematic requires a set of simplification hypotheses associated to high-end mathematical and computational methods. The representation of the mucus with a Bingham fluid has to be seen as a first fundamental step and the general behaviors predicted by the model should be considered as qualitative and non-exhaustive. Nevertheless, the parameterization of the Bingham fluid in our work is consistent with acknowledged mucus properties and our predictions should bring behaviors consistent with the physiology.

Second, our model is based on the hypothesis that the Bingham fluid is of quasi–homogeneous thickness along the airway tree. This hypothesis is crucial to get first analytical insights into the role of surface tension on the behavior of a Bingham fluid layer. However, it appears that the mucus layer thickness presents a degree of variation along the bronchial tree [27]. In addition to global variations, local variations of mucus thickness and airway wall geometry could induce large curvature changes. Consequently, a variation of the fluid motion would develop due to the more complex distribution of the curvature gradients. Nevertheless, as shown in this work, this mucus displacement would tend to smooth, and possibly flatten, the fluid layer.

Hence, by showing that surface tension gradients are able to move overly thick layers of Bingham fluid in airways bifurcations, this work represents a first major step toward the study of the role of the surface tension on mucus movement in the bronchial tree. Further studies should focus on using more realistic airways geometries and shape for the air–mucus interface.

ACKNOWLEDGMENTS

This work has been supported by the Mission pour l'interdisciplinarité du CNRS, the Agence Nationale de la Recherche (the VirtualChest project, ANR-16-CE19-0014; the IDEX UCA JEDI, ANR-15-IDEX-01), the Académie des Systèmes Complexes de l'Université Côte d'Azur and the association Vaincre La Mucoviscidose.

[1] E. R. Weibel, *The Pathway for Oxygen: Structure and Function in the Mammalian Respiratory System* (Harvard University Press, 1984).

[2] J. B. West, *Respiratory Physiology: The Essentials*, 9th ed. (Lippincott Williams and Wilkins, Philadelphia, 2011).

[3] J. V. Fahy and B. F. Dickey, Airway Mucus Function and Dysfunction, The New England journal of medicine **363**, 2233 (2010).

[4] M. King, Physiology of mucus clearance, Paediatric Respiratory Reviews **7**, S212 (2006).

[5] X. M. Bustamante-Marin and L. E. Ostrowski, Cilia and Mucociliary Clearance, Cold Spring Harb Perspect Biol **9**, 10.1101/cshperspect.a028241 (2017).

[6] P. T. MacKlem, Physiology of Cough, Ann Otol Rhinol Laryngol **83**, 761 (1974), publisher: SAGE Publications Inc.

[7] P. J. Basser, T. A. McMahon, and P. Griffith, The mechanism of mucus clearance in cough, Journal of biomechanical engineering **111**, 288 (1989).

[8] J. Stéphano and B. Mauroy, Wall shear stress distribution in a compliant airway tree, Physics of Fluids **33**, 031907 (2021), publisher: American Institute of Physics.

[9] M. Del Donno, D. Bittesnich, A. Chetta, D. Olivieri, and M. T. Lopez-Vidriero, The effect of inflammation on mucociliary clearance in asthma: an overview, Chest **118**, 1142 (2000).

[10] M. Robinson and P. T. B. Bye, Mucociliary clearance in cystic fibrosis, Pediatr Pulmonol **33**, 293 (2002).

[11] J. T. Ito, D. Ramos, F. M. M. Rodrigues, R. F. Xavier, M. R. Leite, J. Nicolino, G. N. B. Ferrari, A. C. Toledo, and E. M. C. Ramos, Impairment of mucociliary clearance in COPD and smokers: Same or different?, European Respiratory Journal **40** (2012), publisher: European Respiratory Society Section: 6.3 Tobacco, Smoking Control and Health Education.

[12] J. M. Zahm, M. King, C. Duvivier, D. Pierrot, S. Girod, and E. Puchelle, Role of simulated repetitive coughing in mucus clearance, European Respiratory Journal **4**, 311 (1991).

[13] B. Mauroy, C. Fausser, D. Pelca, J. Merckx, and P. Flaud, Toward the modeling of mucus draining from the human lung: role of the geometry of the airway tree, Physical Biology **8**, 056006 (2011).

[14] B. Mauroy, P. Flaud, D. Pelca, C. Fausser, J. Merckx, and B. R. Mitchell, Toward the modeling of mucus draining from human lung: role of airways deformation on air-mucus interaction, Front. Physiol. **6**, 10.3389/fphys.2015.00214 (2015).

[15] C. Karamaoun, B. Sobac, B. Mauroy, A. V. Muylem, and B. Haut, New insights into the mechanisms controlling the bronchial mucus balance, PLOS ONE **13**, e0199319 (2018).

[16] L. Xu and Y. Jiang, Mathematical Modeling of Mucociliary Clearance: A Mini-Review, Cells **8**, 736 (2019), number: 7 Publisher: Multidisciplinary Digital Publishing Institute.

[17] J. Stéphano and B. Mauroy, Modeling shear stress distribution in a deformable airway tree, in *27th Canadian Congress of Applied Mechanics* (Sherbrooke, Canada, 2019).

[18] S. Gsell, E. Loiseau, U. D'Ortona, A. Viallat, and J. Favier, Hydrodynamic model of directional ciliary-beat organization in human airways, Scientific Reports **10**, 8405 (2020), number: 1 Publisher: Nature Publishing Group.

[19] P.-G. de Gennes, F. Brochard-Wyart, and D. Quéré, *Capillarity and Wetting Phenomena: Drops, Bubbles, Pearls, Waves* (Springer New York, New York, NY, 2004).

[20] M. Manolidis, D. Isabey, B. Louis, J. B. Grotberg, and M. Filoche, A Macroscopic Model for Simulating the Mucociliary Clearance in a Bronchial Bifurcation: The Role of Surface Tension, Journal of Biomechanical Engineering **138**, 121005 (2016).

[21] E. R. Weibel, A. F. Cournand, and D. W. Richards, *Morphometry of the Human Lung*, 1st ed. (Springer, 1963).

[22] B. Mauroy, M. Filoche, E. R. Weibel, and B. Sapoval, An optimal bronchial tree may be dangerous, Nature **427**, 633 (2004).

[23] M. H. Tawhai, P. Hunter, J. Tschirren, J. Reinhardt, G. McLennan, and E. A. Hoffman, CT-based geometry analysis and finite element models of the human and ovine bronchial tree, J. Appl. Physiol. **97**, 2310 (2004).

[24] B. Sobac, C. Karamaoun, B. Haut, and B. Mauroy, Allometric scaling of heat and water exchanges in the mammals' lung, arXiv:1911.11700 [physics] (2019), arXiv: 1911.11700.

[25] F. Noël, C. Karamaoun, J. A. Dempsey, and B. Mauroy, The origin of the allometric scaling of lung's ventilation in mammals, arXiv:2005.12362 [q-bio] **in revision in PCI MCB** (2020), arXiv: 2005.12362.

[26] S. K. Lai, Y.-Y. Wang, D. Wirtz, and J. Hanes, Micro- and macrorheology of mucus, Advanced Drug Delivery Reviews **61**, 86 (2009).

[27] C. Karamaoun, B. Sobac, B. Mauroy, A. Van Muylem, and B. haut, New analysis of the mechanisms controlling the bronchial mucus balance, in *27th Canadian Congress of Applied Mechanics* (Sherbrooke,, Canada, 2019).

[28] R. Hamed and J. Fiegel, Synthetic Tracheal Mucus with Native Rheological and Surface Tension Properties, J Biomed Mater Res A **102**, 1788 (2014).

[29] G. R. Fulford and J. R. Blake, Muco-ciliary transport in the lung, Journal of Theoretical Biology **121**, 381 (1986).

[30] R. L. Panton, Incompressible Flow, in *Incompressible Flow* (Wiley-Blackwell, 2013) pp. 198–219.

[31] N. J. Balmforth and R. V. Craster, A consistent thin-layer theory for Bingham plastics, Journal of Non-Newtonian Fluid Mechanics **84**, 65 (1999).

[32] J. B. Grotberg, Respiratory Fluid Mechanics and Transport Processes, Annual Review of Biomedical Engineering **3**, 421 (2001).

[33] I. Balásházy, W. Hofmann, and T. Heistracher, Local particle deposition patterns may play a key role in the development of lung cancer, Journal of Applied Physiology **94**, 1719 (2003), publisher: American Physiological Society.

[34] J. R. Zierenberg, D. Halpern, M. Filoche, B. Sapoval, and J. B. Grotberg, An asymptotic model of particle deposition at an airway bifurcation, Mathematical Medicine and Biology: A Journal of the IMA **30**, 131 (2013), conference Name: Mathematical Medicine and Biology: A Journal of the IMA.

[35] B. Mauroy, M. Filoche, J. S. Andrade, and B. Sapoval, Interplay between geometry and flow distribution in an airway tree, Physical Review Letters **90**, 148101 (2003).

[36] C. Geuzaine and J.-F. Remacle, Gmsh: A 3-D finite element mesh generator with built-in pre-and post-processing facilities, International Journal for Numerical Methods in Engineering **79**, 1309 (2009).

[37] F. Guichard, L. Moisan, and J.-M. Morel, A review of P.D.E. models in image processing and image analysis, J. Phys. IV France **12**, 137 (2002), publisher: EDP Sciences.

Appendix

Appendix A: Analysis in a fractal tree

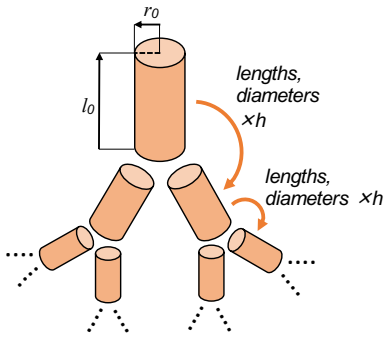

FIG. 3. Fractal model of the bronchial tree used in the qualitative analysis. The size of the branches is decreasing at each bifurcation by a factor $h = (1/2)^{\frac{1}{3}}$. The radius and length of the root of the tree (trachea) are respectively r_0 and l_0.

We search for a qualitative estimation of the pressures induced by surface tension in the generations of the airway tree. The geometry of the bronchial tree is approximated with a cascade of bifurcating cylindrical airways [22, 35], see Fig. 3. The airways are numbered by using a generation index i that represents the number of bifurcations from the root of the tree, i.e. the trachea, to the considered airway. We assume that the dimensions of the airways between two consecutive generations are related by a homothetic factor h, independent of the generation index. The theoretical value $h = (1/2)^{1/3} \simeq 0.79$ has been found to represent adequately the geometry of the mammal lung [1, 21–25].

We assume that the mucus layer in this geometry has a negligible thickness relatively to the airways radii [1, 27]. Then, the principal curvatures of the air–Bingham fluid interface in the generation i can be assimilated to the cylindrical airway principal curvatures: $1/r_i$ in the radial direction and 0 in the axial direction. These curvatures induce a Laplace pressure drop $p_{L,i}$ between the air and the Bingham fluid that formulates into

$$p_{L,i} = -\frac{\gamma}{r_i}$$

Since the airways are considered as perfect cylinders, within a single bronchus, the radius does not vary, no gradient of Laplace pressure is developing and no mass of fluid is transported. However, the radii vary between airways, as the distal (deep) bronchi are smaller than the proximal (upper) ones. Because of this change of curvature, the amplitude of the pressure drop increases with the generation index. This implies that a pressure gradient exists between two successive generations, which are connected through bifurcations.

Between two successive generations i and $i+1$, the radii r_i and r_{i+1} relate as $r_{i+1} = h \times r_i$. Assuming that the length of the bifurcation Δx is of the order of magnitude of the airway radius, the curvature radius gradient between two successive generations can be approximated by $\frac{\Delta r_i}{\Delta x} \simeq \frac{h \times r_i - r_i}{r_i} = (h-1) < 0$. Hence, as in [13], the mean shear stress applied to the layer by the pressure drop between two successive generations i and $i+1$ can be qualitatively evaluated to

$$\sigma \simeq \frac{\Delta p_{L,i}}{\Delta x}\frac{\tau}{2} \simeq \gamma \frac{h-1}{r_0^2 h^{2i}}\frac{\tau}{2} < 0$$

If this stresses overcomes the yield stress σ_y, the Bingham fluid will start to flow. Because Σ_{rx} is negative, the Bingham fluid should flow toward the distal regions of the tree, opposite to the direction of the mucociliary clearance.

The previous analysis suggests that the Laplace pressure gradients should be stronger in the distal bifurcations than in the proximal bifurcations. However, a more refined analysis is needed in order to get proper estimations of those gradients and to determine if they can induce shear stresses high enough to overcome the yield stress of the Bingham fluid.

Appendix B: Lubrication theory, Bingham case

1. Local coordinates system

Coordinates change.
In order to derive the main components of the velocity in the Bingham layer, we will use a lubrication technic based on the hypothesis that the thickness of the layer τ is far smaller than the characteristic length of the domain [31]. This characteristic length is estimated using the characteristic curvature radius R of the surface on which the layer spreads. Typically, this characteristic curvature radius corresponds to the radius of the airway considered.

The first step is to use a local coordinates system. We will denote (x, y, z) the physical coordinates and (ξ_1, ξ_2, ξ_3) the local coordinates system, as schematized in Fig. 4.

$$(x, y, z) \longrightarrow (\xi_1, \xi_2, \xi_3)$$

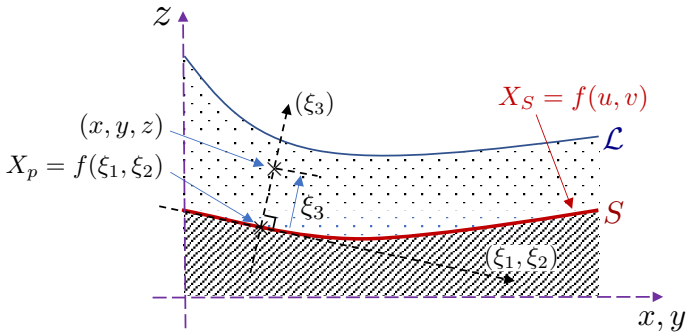

FIG. 4. Transformation from global coordinates $X = (x, y, z)$ to local coordinates $\xi = (\xi_1, \xi_2, \xi_3)$. The plane $(\xi_1\xi_2)$ is tangent to the wall S defined by the surface $X_S = f(u, v)$, where (u, v) is a set of curvilinear coordinates. The direction (ξ_3) is normal to S. The surface $\mathcal{L}$ represents the air–Bingham fluid interface.

We will consider a thin layer that stands on a substrate which surface S can be represented locally with a parametric representation $X_S = f(u, v)$ where $(u, v) \in \Omega$ is a curvilinear parameterization of the surface, with Ω a subset of $\mathbb{R}^2$. In this case, we can project a point $X = (x, y, z)$ in the layer onto the substrate surface, see Fig. 4. The resulting projection point on the surface is denoted $X_p = f(\xi_1, \xi_2)$. Then,

$$X = f(\xi_1, \xi_2) + \xi_3 \, \mathbf{n}_S$$

with

$$\mathbf{n}_S = \left(\frac{\partial f}{\partial u} \wedge \frac{\partial f}{\partial v} \right) / \left\| \frac{\partial f}{\partial u} \wedge \frac{\partial f}{\partial v} \right\|$$

The new coordinates system is then determined by the triplet $\xi = (\xi_1, \xi_2, \xi_3)$.

We will now use a dimensionless formulation of the equations in order to characterize the dominant dynamics of the mucus when $\epsilon = \tau/R$ is small relatively to 1. The ratio ϵ represents the relative thickness of the mucus layer to the curvature of the airways.

We define dimensionless coordinates associated to the triplet $\xi = (\xi_1, \xi_2, \xi_3)$ using the new triplet $\tilde{\xi} = (\tilde{\xi}_1, \tilde{\xi}_2, \tilde{\xi}_3)$ with $\xi_1 = R\tilde{\xi}_1$, $\xi_2 = R\tilde{\xi}_2$ and $\xi_3 = \tau\tilde{\xi}_3$. In the following, the notation with a tilde over a letter indicates a dimensionless quantity.

- Since f defines the airway wall, we assume that the characteristic size of f is also R and we define $\tilde{f}$ as $f = R\tilde{f}$.
- The Laplace pressure is normalized based on $P = \frac{\gamma}{R}$ and $\tilde{p}_L = p_L/P$. Moreover, for Newtonian fluid, velocity is proportional to $\frac{\gamma}{\mu}\epsilon^2$, hence we choose the scaling $U = \frac{\gamma}{\mu}\epsilon^2$ for velocity in ξ_1 and ξ_2 directions. In the ξ_3 direction, the scaling is $W = U\tau/R = U\epsilon$.
- Stresses are rescaled with $\sigma^{*3} = \mu\frac{U}{\tau}\tilde{\sigma}^{*3}$ for $* = 1$ or 2, and the other components are rescaled with $\sigma_* = \mu\frac{U}{R}\tilde{\sigma}*$ for $* = 11$, 22, 33 and 12. We denote $\Sigma_{i,j}$ the rescaling value of σ^{ij}.
- Strains are rescaled accordingly, i.e. as σ/μ.

- We assume that all dimensionless variables can decompose into a series relatively to ϵ, i.e. for a variable $*$, its development writes $* = *_0\ \epsilon^0 + *_1\ \epsilon + *_2\ \epsilon^2 + ...$

2. Metric

We define the matrix $C = (c_{i,j})_{i,j} = (\mathbf{b}_1, \mathbf{b}_2, \mathbf{b}_3)$ with

$$\begin{array}{l} \mathbf{b}_1 = \frac{\partial X}{\partial \xi_1} = \frac{\partial f}{\partial u} + \xi_3 \frac{\partial \mathbf{n}_S}{\partial u} = \frac{\partial \tilde{f}}{\partial \tilde{u}} + \epsilon \tilde{\xi}_3 \frac{\partial \mathbf{n}_S}{\partial \tilde{u}} \\ \mathbf{b}_2 = \frac{\partial X}{\partial \xi_2} = \frac{\partial f}{\partial v} + \xi_3 \frac{\partial \mathbf{n}_S}{\partial v} = \frac{\partial \tilde{f}}{\partial \tilde{v}} + \epsilon \tilde{\xi}_3 \frac{\partial \mathbf{n}_S}{\partial \tilde{v}} \\ \mathbf{b}_3 = \frac{\partial X}{\partial \xi_3} = \mathbf{n}_S \end{array}$$

and the matrix $\bar{C} = (\bar{c}_{i,j})_{i,j} = C^{-1} = (\mathbf{b}^1, \mathbf{b}^2, \mathbf{b}^3)$. We denote C^0 and $\tilde{C}^0$ the first term of the development of C and $\tilde{C}$ in ϵ.

The associated metric tensor is defined with $g_{(i,j)} = (\mathbf{b}_i.\mathbf{b}_j)_{i,j}$ and its inverse with $g^{(i,j)} = (\mathbf{b}^i.\mathbf{b}^j)_{i,j}$. The metric tensors can be rewritten in dimensionless coordinates:

$$g_{(i,j)}(\xi_1, \xi_2, \xi_3) = \tilde{g}_{(i,j)}(\tilde{\xi}_1, \tilde{\xi}_2, \tilde{\xi}_3) = \begin{pmatrix} \left\| \frac{\partial \tilde{f}}{\partial \tilde{u}} \right\|^2 & \frac{\partial \tilde{f}}{\partial \tilde{u}} . \frac{\partial \tilde{f}}{\partial \tilde{v}} & 0 \\ \frac{\partial \tilde{f}}{\partial \tilde{u}} . \frac{\partial \tilde{f}}{\partial \tilde{v}} & \left\| \frac{\partial \tilde{f}}{\partial \tilde{v}} \right\|^2 & 0 \\ 0 & 0 & 1 \end{pmatrix} + O(\epsilon)$$

and

$$g^{(i,j)}(\xi_1, \xi_2, \xi_3) = \tilde{g}^{(i,j)}(\tilde{\xi}_1, \tilde{\xi}_2, \tilde{\xi}_3) = \frac{1}{\tilde{d}(\tilde{u}, \tilde{v})} \begin{pmatrix} \left\| \frac{\partial \tilde{f}}{\partial \tilde{u}} \right\|^2 & -\frac{\partial \tilde{f}}{\partial \tilde{u}} . \frac{\partial \tilde{f}}{\partial \tilde{v}} & 0 \\ -\frac{\partial \tilde{f}}{\partial \tilde{u}} . \frac{\partial \tilde{f}}{\partial \tilde{v}} & \left\| \frac{\partial \tilde{f}}{\partial \tilde{v}} \right\|^2 & 0 \\ 0 & 0 & \tilde{d}(\tilde{u}, \tilde{v}) \end{pmatrix} + O(\epsilon)$$

with $\tilde{d}(\tilde{u}, \tilde{v})$ the determinant of the first term $\tilde{C}^0$ of the development in series of the matrix $\tilde{C}$, $\tilde{d}(\tilde{u}, \tilde{v}) = \left\| \frac{\partial \tilde{f}}{\partial \tilde{u}} \right\|^2 \left\| \frac{\partial \tilde{f}}{\partial \tilde{v}} \right\|^2 - \left(\frac{\partial \tilde{f}}{\partial \tilde{u}} . \frac{\partial \tilde{f}}{\partial \tilde{v}} \right)^2$.

For the sake of notation simplicity, we assume in the following that g^{ij}, g_{ij}, $\tilde{g}^{ij}$ and $\tilde{g}_{ij}$ refer to the term of first order in their development relatively to ϵ.

3. Christoffel symbols of the second kind

The Christoffel symbols of the second kind Γ^j_{ik} allow to compute the derivatives in the local coordinates system (ξ_1, ξ_2, ξ_3). The symbols are written, using Einstein notation,

$$\Gamma^k_{ij} = \frac{1}{2} g^{ip} \left(\frac{\partial g_{pj}}{\partial \xi_k} + \frac{\partial g_{pk}}{\partial \xi_j} - \frac{\partial g_{jk}}{\partial \xi_p} \right)$$

We define normalized versions of the Christoffel symbols according to the dimensionless coordinates defined above:

$$\tilde{\Gamma}^k_{i,j} = R\ \Gamma^k_{i,j}$$

The terms in ϵ^0 in the developments in series of the metric tensors $\tilde{g}^{(i,j)}$ and $\tilde{g}_{(i,j)}$ do not depend on $\tilde{\xi}_3$ and have several null terms in their expression Moreover, we have $g_{3,3} = 1$. With these properties, we can get information on the developments in series of the Christoffel symbols relatively to ϵ:

$$\begin{array}{l} \tilde{\Gamma}^k_{i,j} = O(\epsilon) \ \text{ if at least one of } i,\ j \text{ or } k \text{ is equal to 3} \\ \tilde{\Gamma}^k_{i,j} = O(1) \ \text{ otherwise} \end{array} \tag{B1}$$

4. Equations of the mucus dynamics

We assume that the layer stands on the airway wall S. The air–fluid interface is denoted $\mathcal{L}$. The mucus dynamics equations in the coordinates frame (x, y, z) are

$$\begin{cases} \rho\frac{\partial \mathbf{u}}{\partial t} - \nabla.\Sigma = \nabla p & \text{in the layer} \\ \nabla.\mathbf{u} = 0 & \text{in the layer} \\ \Sigma.\mathbf{n} - p\,\mathbf{n} = p_L\,\mathbf{n} & \text{at the air–fluid interface } \mathcal{L} \\ \mathbf{u} = 0 & \text{on the airway wall } S \\ \frac{\partial \mathbf{X}_\mathcal{L}}{\partial t} = (\mathbf{u}(\mathbf{X}_\mathcal{L}).\mathbf{n})\,\mathbf{n} & \text{at the air–fluid interface } \mathcal{L}, \text{ for } \mathbf{X}_\mathcal{L} \in \mathcal{L} \\ p_L = -2\gamma\kappa(x, y, z, t) & \text{at the air–fluid interface } \mathcal{L} \end{cases} \tag{B2}$$

We decompose these equations in the coordinates system $(\mathbf{b}_1, \mathbf{b}_2, \mathbf{b}_3)$. The coordinates of the velocity u in that frame is (u^1, u^2, u^3). The covariant differentiation of a quantity $*$ relatively to the coordinate on the component b_j is denoted $*_{,j}$, and

$$\begin{aligned} p_{,j} &= g^{ji}\frac{\partial p}{\partial \xi_i} \\ \mathrm{div}_{co}\,\Sigma &= \sum_{j=1}^{3}\left(\frac{\partial \sigma^{ij}}{\partial \xi_i} + \Gamma^i_{il}\sigma^{lj} + \Gamma^j_{il}\sigma^{il}\right) b_j \\ \frac{\partial u}{\partial t} &= \sum_{j=1}^{3}\frac{\partial u^j}{\partial t} b_j \end{aligned}$$

For any $j \in \{1, 2, 3\}$, the component of the equation on $\mathbf{b}_j$ is

$$\rho\frac{\partial u^j}{\partial t} - \left(\frac{\partial \sigma^{ij}}{\partial \xi_i} + \Gamma^i_{il}\sigma^{lj} + \Gamma^j_{il}\sigma^{il}\right) + g^{ji}\frac{\partial p}{\partial \xi_i} = 0$$

Finally, we can write the stress tensor as

$$\Sigma = \frac{\mu U}{R}\tilde{\Sigma} \quad \text{with} \quad \tilde{\Sigma} = \begin{pmatrix} \tilde{\sigma}^{11} & \tilde{\sigma}^{12} & \frac{1}{\epsilon}\tilde{\sigma}^{13} \\ \tilde{\sigma}^{12} & \tilde{\sigma}^{22} & \frac{1}{\epsilon}\tilde{\sigma}^{23} \\ \frac{1}{\epsilon}\tilde{\sigma}^{13} & \frac{1}{\epsilon}\tilde{\sigma}^{23} & \tilde{\sigma}^{33} \end{pmatrix} \tag{B3}$$

5. Air–mucus interface $\mathcal{L}$

The air–mucus interface is defined in the coordinates system (ξ_1, ξ_2, ξ_3) as

$$\mathcal{L} = \{X_\mathcal{L} = g(u, v) = f(u, v) + \tau\,(1 + \eta(u, v, t))\,\mathbf{n}_S(u, v)\,|(u, v) \in \Omega\,\}$$

where η is a function from Ω such that $\eta = o\left(\frac{1}{\epsilon}\right)$, i.e. $\epsilon \times \eta \underset{\epsilon\to 0}{\longrightarrow} 0$. Hence, the order of magnitude of η is at most 1. Moreover, we assume that the layer cannot be of negative thickness and $\eta \geq -1$.

The normal of the air–mucus interface can then be defined as

$$\mathbf{n}_\mathcal{L} = \left(\frac{\partial g}{\partial u} \wedge \frac{\partial g}{\partial v}\right) \Big/ \left|\left|\frac{\partial g}{\partial u} \wedge \frac{\partial g}{\partial v}\right|\right|$$

Using the dimensionless system of coordinates, we normalize g with $\tilde{g}(\tilde{\xi_1}, \tilde{\xi_2}, \tilde{\xi_3}) = g(\xi_1, \xi_2, \xi_3)/R$ and we denote $\tilde{\mathbf{n}}_*(\tilde{\xi_1}, \tilde{\xi_2}, \tilde{\xi_3}) = \mathbf{n}_*(\xi_1, \xi_2, \xi_3)$ with $* = \mathcal{L}$ or S. We can then deduce that

$$\tilde{\mathbf{n}}_\mathcal{L} = \tilde{\mathbf{n}}_S + \underbrace{\epsilon\,(1 + \tilde{\eta})\frac{\frac{\partial \tilde{f}}{\partial \tilde{u}} \wedge \frac{\partial \mathbf{n}_S}{\partial \tilde{v}} - \frac{\partial \tilde{f}}{\partial \tilde{v}} \wedge \frac{\partial \mathbf{n}_S}{\partial \tilde{u}}}{\left|\left|\frac{\partial f}{\partial u} \wedge \frac{\partial f}{\partial v}\right|\right|}}_{\tilde{\mathbf{m}}_\mathcal{L}} + O(\epsilon^2) \tag{B4}$$

with $\tilde{\eta}(\tilde{\xi_1}, \tilde{\xi_2}, \tilde{t}) = \eta(\xi_1, \xi_2, t)$.

The air–mucus interface is a surface of equation $\xi_3 = \tau(1 + \eta(\xi_1, \xi_2))$ or, in dimensionless coordinates, $\tilde{\xi_3} = 1 + \tilde{\eta}(\tilde{\xi_1}, \tilde{\xi_2})$.

6. Boundary conditions at the air–mucus interface $\mathcal{L}$

Based on equation (B4), the boundary condition $\Sigma.\mathbf{n}_{\mathcal{L}} - p.\mathbf{n}_{\mathcal{L}} = -p_L.\mathbf{n}_{\mathcal{L}}$ at the air–mucus interface becomes in the dimensionless formulation

$$\tilde{\Sigma}.\tilde{\mathbf{n}}_{\mathcal{L}} - \frac{1}{\epsilon^2}\tilde{p}.\tilde{\mathbf{n}}_{\mathcal{L}} = -\frac{1}{\epsilon^2}\tilde{p}_L.\tilde{\mathbf{n}}_{\mathcal{L}}$$

Then, based on the expression of $\tilde{\Sigma}$ in equation (B3) and of the normal at the air–mucus interface in equation (B4), $\tilde{\mathbf{n}}_{\mathcal{L}} = \tilde{\mathbf{n}}_S + \epsilon\ \tilde{\mathbf{m}}_{\mathcal{L}} + O(\epsilon^2)$, we can derive the following relationships,

- At the order $\frac{1}{\epsilon^2}$: $\tilde{p}^0(\xi_1, \xi_2, 1 + \tilde{\eta}(\xi_1, \xi_2, \tilde{t})) = \tilde{p}_L(\xi_1, \xi_2)$.
- At the order $\frac{1}{\epsilon}$: The boundary condition at $\tilde{\xi}_3 = 1 + \eta(\tilde{\xi}_1, \tilde{\xi}_2, \tilde{t})$ is, at the order $1/\epsilon$:

$$\begin{pmatrix} 0 & 0 & \tilde{\sigma}_0^{13} \\ 0 & 0 & \tilde{\sigma}_0^{23} \\ \tilde{\sigma}_0^{13} & \tilde{\sigma}_0^{23} & 0 \end{pmatrix}.\tilde{\mathbf{n}}_S - p_1\tilde{\mathbf{n}}_S - p_0\tilde{\mathbf{m}}_L = p_L\tilde{\mathbf{m}}_L$$

  Since $p_0 = p_L$ on the boundary and since, in the coordinate system $(\tilde{\xi}_1, \tilde{\xi}_2, \tilde{\xi}_3)$, $\tilde{\mathbf{n}}_S = {}^t(0, 0, 1)$, we can conclude that

$$\begin{aligned} &\tilde{\sigma}_0^{13}\left(\tilde{\xi}_1, \tilde{\xi}_2, 1 + \tilde{\eta}(\tilde{\xi}_1, \tilde{\xi}_2, \tilde{t}), \tilde{t}\right) = \tilde{\sigma}_0^{23}\left(\tilde{\xi}_1, \tilde{\xi}_2, 1 + \tilde{\eta}(\tilde{\xi}_1, \tilde{\xi}_2, \tilde{t}), \tilde{t}\right) = 0 \\ &\tilde{\sigma}_0^{33}\left(\tilde{\xi}_1, \tilde{\xi}_2, 1 + \tilde{\eta}(\tilde{\xi}_1, \tilde{\xi}_2, \tilde{t}), \tilde{t}\right) - \tilde{p}_1 = 0 \end{aligned} \tag{B5}$$

7. Component along $\mathbf{b_3}$

On the component $\mathbf{b}_3$, the equations reduce to

$$\rho\frac{\partial u^3}{\partial t} - \left(\frac{\partial \sigma^{i3}}{\partial \xi_i} + \Gamma^i_{il}\sigma^{l3} + \Gamma^3_{il}\sigma^{il}\right) + g^{3i}\frac{\partial p}{\partial \xi_i} = 0$$

Then, using $g^{31} = g^{32} = 0$ and $g^{33} = 1$ and formulating the equations in a dimensionless form, we have

$$\begin{aligned} \frac{\rho W}{T}\frac{\partial \tilde{u}^3}{\partial \tilde{t}} &- \left(\frac{\Sigma^{13}}{R}\frac{\partial \tilde{\sigma}^{13}}{\partial \tilde{\xi}_1} + \frac{\Sigma^{l3}}{R}\ \tilde{\Gamma}^1_{1l}\tilde{\sigma}^{l3} + \frac{\Sigma^{1l}}{R}\ \tilde{\Gamma}^3_{1l}\tilde{\sigma}^{1l}\right) \\ &- \left(\frac{\Sigma^{23}}{R}\frac{\partial \tilde{\sigma}^{23}}{\partial \tilde{\xi}_2} + \frac{\Sigma^{l3}}{R}\ \tilde{\Gamma}^2_{2l}\tilde{\sigma}^{l3} + \frac{\Sigma^{2l}}{R}\ \tilde{\Gamma}^3_{2l}\tilde{\sigma}^{2l}\right) \\ &- \left(\frac{\Sigma^{33}}{\tau}\frac{\partial \tilde{\sigma}^{33}}{\partial \tilde{\xi}_3} + \frac{\Sigma^{l3}}{R}\ \tilde{\Gamma}^3_{3l}\tilde{\sigma}^{l3} + \frac{\Sigma^{3l}}{R}\ \tilde{\Gamma}^3_{3l}\tilde{\sigma}^{3l}\right) + \frac{P}{\tau}\frac{\partial \tilde{p}}{\partial \tilde{\xi}_3} = 0 \end{aligned} \tag{B6}$$

or, once multiplied by $\frac{R^2}{\mu U}$ for getting dimensionless coefficients in front of the derivatives,

$$\begin{aligned} \overbrace{\frac{\rho R^2}{\mu T}}^{\substack{\text{fixed to 1} \\ \text{with } T = \frac{\rho R^2}{\mu}}} &\frac{1}{\epsilon}\frac{\partial \tilde{u}^3}{\partial \tilde{t}} - \left(\frac{1}{\epsilon}\frac{\partial \tilde{\sigma}^{13}}{\partial \tilde{\xi}_1} + \frac{1}{\epsilon}\ \tilde{\Gamma}^1_{11}\tilde{\sigma}^{13} + \tilde{\Gamma}^3_{11}\tilde{\sigma}^{11} + \frac{1}{\epsilon}\ \tilde{\Gamma}^1_{12}\tilde{\sigma}^{23} + \tilde{\Gamma}^3_{12}\tilde{\sigma}^{12} + \tilde{\Gamma}^1_{13}\tilde{\sigma}^{33} + \frac{1}{\epsilon}\ \tilde{\Gamma}^3_{13}\tilde{\sigma}^{13}\right) \\ &- \left(\frac{1}{\epsilon}\frac{\partial \tilde{\sigma}^{23}}{\partial \tilde{\xi}_2} + \frac{1}{\epsilon}\ \tilde{\Gamma}^2_{21}\tilde{\sigma}^{13} + \tilde{\Gamma}^3_{21}\tilde{\sigma}^{21} + \frac{1}{\epsilon}\ \tilde{\Gamma}^2_{22}\tilde{\sigma}^{23} + \tilde{\Gamma}^3_{22}\tilde{\sigma}^{22} + \tilde{\Gamma}^2_{23}\tilde{\sigma}^{33} + \frac{1}{\epsilon}\ \tilde{\Gamma}^3_{23}\tilde{\sigma}^{23}\right) \\ &- \left(\frac{1}{\epsilon}\frac{\partial \tilde{\sigma}^{33}}{\partial \tilde{\xi}_3} + \frac{1}{\epsilon}\ \tilde{\Gamma}^3_{31}\tilde{\sigma}^{13} + \frac{1}{\epsilon}\ \tilde{\Gamma}^3_{31}\tilde{\sigma}^{31} + \frac{1}{\epsilon}\ \tilde{\Gamma}^3_{32}\tilde{\sigma}^{23} + \frac{1}{\epsilon}\ \tilde{\Gamma}^3_{32}\tilde{\sigma}^{32} + 2\tilde{\Gamma}^3_{33}\tilde{\sigma}^{33}\right) + \underbrace{\frac{PR}{\mu U}}_{=1/\epsilon^2}\frac{1}{\epsilon}\frac{\partial \tilde{p}}{\partial \tilde{\xi}_3} = 0 \end{aligned} \tag{B7}$$

Since we have shown that all the dimensionless Christoffel symbols are at least $O(1)$ in ϵ, the equations at the order ϵ^{-3} reduce to $\frac{\partial \tilde{p}_0}{\partial \tilde{\xi}_3} = 0$, where $\tilde{p}_0$ is the term in ϵ^0 of the development in series relatively to ϵ of $\tilde{p}$. Then, using the boundary condition on the pressure in equation (1),

$$\tilde{p}_0(\tilde{\xi}_1, \tilde{\xi}_2, \tilde{\xi}_3, \tilde{t}) = \tilde{p}_0(\tilde{\xi}_1, \tilde{\xi}_2, 1 + \tilde{\eta}(\tilde{\xi}_1, \tilde{\xi}_2, \tilde{t}), \tilde{t}) = \tilde{p}_L(\xi_1, \xi_2, \tilde{t})$$

At the first order in ϵ, the pressure does not dependent on ξ_3.

At the order ϵ^{-2}, the equations (B7) reduce to $\frac{\partial \tilde{p}_1}{\partial \tilde{\xi}_3} = 0$, where $\tilde{p}_1$ is the term in ϵ^1 of the development in series relatively to ϵ of $\tilde{p}$. And we can conclude that $\tilde{p}_1 = 0$ since $\tilde{p} = p_L$ on the air–mucus interface.

8. Component along $\mathbf{b}_1$

As for the component $\mathbf{b}_3$, the equations on the component $\mathbf{b}_1$ reduce to

$$\rho \frac{\partial u^1}{\partial t} - \left(\frac{\partial \sigma^{i1}}{\partial \xi_i} + \Gamma^i_{il}\sigma^{l1} + \Gamma^1_{il}\sigma^{il} \right) + g^{1i}\frac{\partial p}{\partial \xi_i} = 0$$

Or, in dimensionless coordinates and multiplied by $\frac{R^2}{\mu U}$,

$$\begin{aligned}
&\overbrace{\frac{\rho R^2}{\mu T}}^{=1} \frac{\partial \tilde{u}^1}{\partial \tilde{t}} - \left(\frac{\partial \tilde{\sigma}^{11}}{\partial \tilde{\xi}_1} + \tilde{\Gamma}^1_{11}\tilde{\sigma}^{11} + \tilde{\Gamma}^1_{11}\sigma^{11} + \tilde{\Gamma}^1_{12}\tilde{\sigma}^{21} + \tilde{\Gamma}^1_{12}\sigma^{12} + \frac{1}{\epsilon}\overbrace{\tilde{\Gamma}^1_{13}}^{O(\epsilon)}\tilde{\sigma}^{31} + \frac{1}{\epsilon}\overbrace{\tilde{\Gamma}^1_{13}}^{O(\epsilon)}\sigma^{13} \right) \\
&- \left(\frac{\partial \tilde{\sigma}^{21}}{\partial \tilde{\xi}_2} + \tilde{\Gamma}^2_{21}\tilde{\sigma}^{11} + \tilde{\Gamma}^1_{21}\tilde{\sigma}^{21} + \tilde{\Gamma}^2_{22}\tilde{\sigma}^{21} + \tilde{\Gamma}^1_{22}\tilde{\sigma}^{22} + \frac{1}{\epsilon}\overbrace{\tilde{\Gamma}^2_{23}}^{O(\epsilon)}\tilde{\sigma}^{31} + \frac{1}{\epsilon}\overbrace{\tilde{\Gamma}^1_{23}}^{O(\epsilon)}\tilde{\sigma}^{23} \right) \\
&- \left(\frac{1}{\epsilon^2}\frac{\partial \tilde{\sigma}^{31}}{\partial \tilde{\xi}_3} + \overbrace{\tilde{\Gamma}^3_{31}}^{O(\epsilon)}\tilde{\sigma}^{11} + \frac{1}{\epsilon}\overbrace{\tilde{\Gamma}^1_{31}}^{O(\epsilon)}\sigma^{31} + \overbrace{\tilde{\Gamma}^3_{32}}^{O(\epsilon)}\tilde{\sigma}^{21} + \frac{1}{\epsilon}\overbrace{\tilde{\Gamma}^1_{32}}^{O(\epsilon)}\sigma^{32} + \frac{1}{\epsilon}\overbrace{\tilde{\Gamma}^3_{33}}^{O(\epsilon)}\tilde{\sigma}^{31} + \overbrace{\tilde{\Gamma}^1_{33}}^{O(\epsilon)}\sigma^{33} \right) \\
&+ \underbrace{\frac{PR}{\mu U}}_{=1/\epsilon^2} \left(\tilde{g}^{11}\frac{\partial \tilde{p}}{\partial \tilde{\xi}_1} + \tilde{g}^{12}\frac{\partial \tilde{p}}{\partial \tilde{\xi}_2} \right) = 0
\end{aligned} \tag{B8}$$

Finally, we can extract the term of the equations at the order ϵ^{-2},

$$\frac{\partial \tilde{\sigma}^{31}_0}{\partial \tilde{\xi}_3} = \tilde{g}^{11}\frac{\partial \tilde{p}_0}{\partial \tilde{\xi}_1} + \tilde{g}^{12}\frac{\partial \tilde{p}_0}{\partial \tilde{\xi}_2}$$

where $\tilde{\sigma}^{31}_0$ is the first term of the development in series of $\tilde{\sigma}^{31}$ relatively to ϵ. Since $\tilde{p}_0 = \tilde{p}_L$ does not depend on $\tilde{\xi}_3$, we can integrate the equation using the stress boundary conditions (equation (B5)) at the air–mucus interface, i.e. at $\tilde{\xi}_3 = 1 + \tilde{\eta}(\tilde{\xi}_1, \tilde{\xi}_2)$, and get

$$\tilde{\sigma}^{31}_0(\tilde{\xi}_1, \tilde{\xi}_2, \tilde{\xi}_3, \tilde{t}) = -\overbrace{\left(\tilde{g}^{11}\frac{\partial \tilde{p}_L}{\partial \tilde{\xi}_1} + \tilde{g}^{12}\frac{\partial \tilde{p}_L}{\partial \tilde{\xi}_2} \right)}^{\tilde{\partial}\tilde{p}_{L1}} \left(1 + \tilde{\eta}(\tilde{\xi}_1, \tilde{\xi}_2, \tilde{t}) - \tilde{\xi}_3 \right) \tag{B9}$$

Doing a similar analysis on the component $\mathbf{b}_2$ leads to

$$\tilde{\sigma}^{32}_0(\tilde{\xi}_1, \tilde{\xi}_2, \tilde{\xi}_3, \tilde{t}) = -\underbrace{\left(\tilde{g}^{21}\frac{\partial \tilde{p}_L}{\partial \tilde{\xi}_1} + \tilde{g}^{22}\frac{\partial \tilde{p}_L}{\partial \tilde{\xi}_2} \right)}_{\tilde{\partial}\tilde{p}_{L2}} \left(1 + \tilde{\eta}(\tilde{\xi}_1, \tilde{\xi}_2, \tilde{t}) - \tilde{\xi}_3 \right) \tag{B10}$$

For $i = 1, 2$, we define the operator $\tilde{\partial}\tilde{q}_i$ of a quantity $\tilde{q}$ as

$$\tilde{\partial}\tilde{q}_i = \tilde{g}^{i1}\frac{\partial\tilde{q}}{\partial\tilde{\xi}_1} + \tilde{g}^{i2}\frac{\partial\tilde{q}}{\partial\tilde{\xi}_2}$$

Then, we define the operator $\nabla_{\tilde{\xi}}\,\tilde{q}$ of a quantity $\tilde{q}$ as

$$\nabla_{\tilde{\xi}}\,\tilde{q} = \tilde{\partial}\tilde{q}_1\tilde{\mathbf{b}}_1 + \tilde{\partial}\tilde{q}_2\tilde{\mathbf{b}}_2$$

and $\|\nabla_{\tilde{\xi}}\,\tilde{q}\| = \sqrt{\tilde{g}_{11}(\tilde{\partial}\tilde{q}_1)^2 + \tilde{g}_{22}(\tilde{\partial}\tilde{q}_2)^2 + 2\tilde{g}_{12}\tilde{\partial}\tilde{q}_1\tilde{\partial}\tilde{q}_2}$. Using these notations, we have

$$\tilde{\sigma}_0^{31}(\tilde{\xi}_1,\tilde{\xi}_2,\tilde{\xi}_3,\tilde{t}) = -\tilde{\partial}\tilde{p}_{L1}\left(1+\tilde{\eta}(\tilde{\xi}_1,\tilde{\xi}_2,\tilde{t}) - \tilde{\xi}_3\right)$$
$$\tilde{\sigma}_0^{32}(\tilde{\xi}_1,\tilde{\xi}_2,\tilde{\xi}_3,\tilde{t}) = -\tilde{\partial}\tilde{p}_{L2}\left(1+\tilde{\eta}(\tilde{\xi}_1,\tilde{\xi}_2,\tilde{t}) - \tilde{\xi}_3\right)$$

Moreover, knowing that $\tilde{p}_1 = 0$, the terms in ϵ^{-1} in the equations (B8) and in their equivalent on the component $\mathbf{b}_2$ lead to

$$\frac{\partial\tilde{\sigma}_1^{31}}{\partial\tilde{\xi}_3} = \tilde{g}^{11}\frac{\partial\tilde{p}_1}{\partial\tilde{\xi}_1} + \tilde{g}^{12}\frac{\partial\tilde{p}_1}{\partial\tilde{\xi}_2} = 0$$
$$\frac{\partial\tilde{\sigma}_1^{32}}{\partial\tilde{\xi}_3} = \tilde{g}^{21}\frac{\partial\tilde{p}_1}{\partial\tilde{\xi}_1} + \tilde{g}^{22}\frac{\partial\tilde{p}_1}{\partial\tilde{\xi}_2} = 0$$

Consequently, both $\tilde{\sigma}_1^{31}$ and $\tilde{\sigma}_1^{32}$ are independent on $\tilde{\xi}_3$.

9. Curvature

The local curvature of the air–Bingham interface $\mathcal{L}$ parameterized as $\mathbf{X}_{\mathcal{L}} = g(u,v,t) = f(u,v) + \tau(1+\eta(u,v,t))\mathbf{n}_S(u,v)$ is

$$\kappa(u,v) = \frac{(1+\frac{\partial g}{\partial u}^2)\frac{\partial^2 g}{\partial v^2} - 2\frac{\partial g}{\partial u}\frac{\partial g}{\partial v}\frac{\partial^2 g}{\partial u\partial v} + (1+\frac{\partial g}{\partial v}^2)\frac{\partial^2 g}{\partial u^2}}{(1+\frac{\partial g}{\partial u}^2+\frac{\partial g}{\partial v}^2)^{\frac{3}{2}}}$$

Then, if we denote $\tilde{\kappa}(\tilde{u},\tilde{v}) = R\,\kappa(u,v)$ and use the previously defined dimensionless variables, then

$$\tilde{\kappa}(\tilde{u},\tilde{v}) = \frac{(1+\frac{\partial\tilde{f}}{\partial\tilde{u}}^2)\frac{\partial^2\tilde{f}}{\partial\tilde{v}^2} - 2\frac{\partial\tilde{f}}{\partial\tilde{u}}\frac{\partial\tilde{f}}{\partial\tilde{v}}\frac{\partial^2\tilde{f}}{\partial\tilde{u}\partial\tilde{v}} + (1+\frac{\partial\tilde{f}}{\partial\tilde{v}}^2)\frac{\partial^2\tilde{f}}{\partial\tilde{u}^2}}{(1+\frac{\partial\tilde{f}}{\partial\tilde{u}}^2+\frac{\partial\tilde{f}}{\partial\tilde{v}}^2)^{\frac{3}{2}}} + O(\epsilon)$$

with $f = R\tilde{f}$, $u = R\tilde{u}$, $v = R\tilde{v}$ and $\epsilon = \tau/R$.

10. Model for mucus rheology

We assume a quasi-static response of the surface tension to curvature changes and assume the mucus behaves as a Bingham fluid as in [13, 14]. The Bingham viscoplastic constitutive model is

$$\begin{cases} \Sigma = \left(\mu + \frac{\sigma_y}{\dot{\gamma}}\right)\dot{\Gamma} & \text{for } \sigma > \sigma_y \\ \dot{\Gamma} = 0 & \text{for } \sigma \le \sigma_y \end{cases} \tag{B11}$$

with $\dot{\Gamma} = (\dot{\gamma}_{i,j})_{i,j=1\ldots3} = \frac{1}{2}\left(\nabla u +^t \nabla u\right)$. The quantities σ and $\dot{\gamma}$ are defined as $\sigma = \sqrt{\frac{1}{2}\Sigma{:}\Sigma}$ and $\dot{\gamma} = \sqrt{\frac{1}{2}\dot{\Gamma}{:}\dot{\Gamma}}$.

These quantities are defined in the coordinate system (x, y, z). Their expression in the coordinate system (ξ_1, ξ_2, ξ_3) are obtained by using the covariant differentiation. Hence, in (ξ_1, ξ_2, ξ_3), the derivative relatively to ξ_j of the $\mathbf{b}_i$ component u^i of the velocity is

$$u^i_{,j} = \frac{\partial u_i}{\partial \xi_j} + \sum_{k=1}^{3} \Gamma^i_{jk} u^k \tag{B12}$$

The dimensionless formulation of this derivative is given by the dimensionless velocities $u_i = U\tilde{u}_i$ for $i = 1, 2$ and $u_3 = U\epsilon\tilde{u}_3$. Then the dimensionless formulation of the covariant derivatives are

$$\begin{array}{ll} u^i_{,j} = \frac{U}{R}\tilde{u}^i_{,j} & \text{for } i = 1,2 \text{ and } j = 1,2 \\ u^3_{,j} = \frac{U\epsilon}{R}\tilde{u}^3_{,j} & \text{for } j = 1,2 \\ u^i_{,3} = \frac{U}{\tau}\tilde{u}^i_{,3} & \text{for } i = 1,2 \\ u^3_{,3} = \frac{U\epsilon}{\tau}\tilde{u}^3_{,3} = \frac{U}{R}\tilde{u}^3_{,3} & \end{array}$$

And,

$$\begin{array}{ll} \tilde{u}^i_{,j} = \frac{\partial \tilde{u}^i}{\partial \tilde{\xi}_j} + \underbrace{\tilde{\Gamma}^i_{j1}}_{O(1)}\tilde{u}^1 + \underbrace{\tilde{\Gamma}^i_{j2}}_{O(1)}\tilde{u}^2 + \underbrace{\tilde{\Gamma}^i_{j3}}_{O(\epsilon)}\epsilon\,\tilde{u}^3 = O(1) & \text{for } i = 1,2 \text{ and } j = 1,2 \\ \tilde{u}^3_{,j} = \frac{\partial \tilde{u}^3}{\partial \tilde{\xi}_j} + \underbrace{\tilde{\Gamma}^3_{j1}}_{O(\epsilon)}\tilde{u}^1 + \underbrace{\tilde{\Gamma}^3_{j2}}_{O(\epsilon)}\tilde{u}^2 + \underbrace{\tilde{\Gamma}^3_{j3}}_{O(\epsilon)}\epsilon\,\tilde{u}^3 = O(1) & \text{for } j = 1,2 \\ \tilde{u}^i_{,3} = \frac{1}{\epsilon}\frac{\partial \tilde{u}^i}{\partial \tilde{\xi}_3} + \underbrace{\tilde{\Gamma}^i_{31}}_{O(\epsilon)}\tilde{u}^1 + \underbrace{\tilde{\Gamma}^i_{32}}_{O(\epsilon)}\tilde{u}^2 + \underbrace{\tilde{\Gamma}^i_{33}}_{O(\epsilon)}\epsilon\,\tilde{u}^3 = \frac{1}{\epsilon}\frac{\partial u^i}{\partial \tilde{\xi}_3} + O(\epsilon) & \text{for } i = 1,2 \\ \tilde{u}^3_{,3} = \frac{\partial \tilde{u}^3}{\partial \tilde{\xi}_3} + \underbrace{\tilde{\Gamma}^3_{31}}_{O(\epsilon)}\tilde{u}^1 + \underbrace{\tilde{\Gamma}^3_{32}}_{O(\epsilon)}\tilde{u}^2 + \underbrace{\tilde{\Gamma}^3_{33}}_{O(\epsilon)}\epsilon\,\tilde{u}^3 = O(1) & \end{array} \tag{B13}$$

Moreover, we denote $\dot{\gamma} = \frac{U}{R}\tilde{\dot{\gamma}}$. Then, using the dimensionless Christoffel symbols from equation (B1) and rewriting the covariant derivatives (equation (B12)) in a dimensionless form, we can compute the dominant term in ϵ of the dimensionless shear rate:

$$\tilde{\dot{\gamma}} = \frac{1}{2\epsilon}\overbrace{\tilde{g}_{33}}^{=1}\sqrt{\tilde{g}_{11}\left(\frac{\partial \tilde{u}^1}{\partial \tilde{\xi}_3}\right)^2 + \tilde{g}_{22}\left(\frac{\partial \tilde{u}^2}{\partial \tilde{\xi}_3}\right)^2 + 2\tilde{g}_{12}\frac{\partial \tilde{u}^1}{\partial \tilde{\xi}_3}\frac{\partial \tilde{u}^2}{\partial \tilde{\xi}_3}} + O(1) = \frac{1}{\epsilon}E$$

Similary, for the stress σ with $\sigma = \frac{\mu U}{R}\tilde{\sigma}$,

$$\tilde{\sigma} = \frac{1}{2\epsilon}\overbrace{\tilde{g}_{33}}^{=1}\sqrt{\tilde{g}_{11}\left(\tilde{\sigma}^{13}\right)^2 + \tilde{g}_{22}\left(\tilde{\sigma}^{23}\right)^2 + 2\tilde{g}_{12}\tilde{\sigma}^{13}\tilde{\sigma}^{23}} + O(1) = \frac{1}{\epsilon}T$$

The yield condition $\sigma \geq \sigma_y$ rewrites

$$\tilde{\sigma} \geq \frac{\sigma_y R}{\mu U} = \frac{1}{\epsilon}\frac{\sigma_y \tau}{\mu U} = \frac{1}{\epsilon}\frac{\sigma_y R^2}{\gamma\tau} = \frac{1}{\epsilon}B$$

where $B = \frac{\sigma_y R^2}{\gamma\tau}$ is the Bingham number, that compares the yield stress to the surface tension stress.

Under plastic conditions, i.e. $\epsilon\tilde{\sigma} < B$, we have $\tilde{\dot{\gamma}} = 0$. Under flow conditions, i.e. when $\tilde{\sigma} \geq B/\epsilon$, stress-strain relationships at the order $1/\epsilon$ are

$$\begin{cases} \tilde{\sigma}^{13}_0 = \dfrac{\partial \tilde{u}^1_0}{\partial \tilde{\xi}_3}\left(1 + \dfrac{B}{E^0}\right) = -\tilde{\partial}\tilde{p}_{L1}(1 + \tilde{\eta} - \tilde{\xi}_3) \\ \tilde{\sigma}^{23}_0 = \dfrac{\partial \tilde{u}^2_0}{\partial \tilde{\xi}_3}\left(1 + \dfrac{B}{E^0}\right) = -\tilde{\partial}\tilde{p}_{L2}(1 + \tilde{\eta} - \tilde{\xi}_3) \\ E^0 = \sqrt{\tilde{g}_{11}\left(\dfrac{\partial \tilde{u}^1_0}{\partial \tilde{\xi}_3}\right)^2 + \tilde{g}_{22}\left(\dfrac{\partial \tilde{u}^2_0}{\partial \tilde{\xi}_3}\right)^2 + 2\tilde{g}_{12}\dfrac{\partial \tilde{u}^1_0}{\partial \tilde{\xi}_3}\dfrac{\partial \tilde{u}^2_0}{\partial \tilde{\xi}_3}} \end{cases} \tag{B14}$$

The first two equations show that u_0^1 and u_0^2 are increasing in amplitude with $\tilde{\xi}_3$ since their $\tilde{\xi}_3$ derivative is positive. We also have $\frac{\partial \tilde{u}_0^2}{\partial \tilde{\xi}_3}\ \tilde{\partial}\tilde{p}_{L1} = \frac{\partial \tilde{u}_0^1}{\partial \tilde{\xi}_3}\ \tilde{\partial}\tilde{p}_{L2}$ and $E^0 = |\frac{\partial \tilde{u}_0^1}{\partial \tilde{\xi}_3}|\ ||\nabla_{\tilde{\xi}}\tilde{p}_L||/|\tilde{\partial}\tilde{p}_{L1}| = |\frac{\partial \tilde{u}_0^2}{\partial \tilde{\xi}_3}|\ ||\nabla_{\tilde{\xi}}\tilde{p}_L||/|\tilde{\partial}\tilde{p}_{L2}|$, with $||\nabla_{\tilde{\xi}}\tilde{p}_L||^2 = \tilde{g}_{11}\tilde{\partial}\tilde{p}_{L1}^2 + \tilde{g}_{22}\tilde{\partial}\tilde{p}_{L2}^2 + 2\tilde{g}_{12}\tilde{\partial}\tilde{p}_{L1}\tilde{\partial}\tilde{p}_{L2}$.

As the stress is decreasing with ξ_3, if the fluid is liquid at the height $\tilde{\xi}_3$, then it is liquid at the height 0. Hence, integrating equations (B14) from 0 to $\tilde{\xi}_3$ and adding the boundary conditions (B5) lead to

$$\begin{aligned}\tilde{u}_0^1 &= \frac{1}{2}\tilde{\partial}\tilde{p}_{L1}\ \tilde{\xi}_3\left(\tilde{\xi}_3 - 2\left(1+\tilde{\eta} - \frac{B}{||\nabla_{\tilde{\xi}}\tilde{p}_L||}\right)\right)\\ \tilde{u}_0^2 &= \frac{1}{2}\tilde{\partial}\tilde{p}_{L2}\ \tilde{\xi}_3\left(\tilde{\xi}_3 - 2\left(1+\tilde{\eta} - \frac{B}{||\nabla_{\tilde{\xi}}\tilde{p}_L||}\right)\right)\end{aligned} \tag{B15}$$

The stress is then

$$\tilde{\sigma}_0 = \frac{1}{\epsilon}\sqrt{\tilde{g}_{11}(\tilde{\sigma}_0^{13})^2 + \tilde{g}_{22}(\tilde{\sigma}_0^{23})^2 + 2\tilde{g}_{12}\tilde{\sigma}_0^{13}\tilde{\sigma}_0^{23}} = \frac{|1+\tilde{\eta}-\tilde{\xi}_3|}{\epsilon} \times ||\nabla_{\tilde{\xi}}\tilde{p}_L||$$

The fluid is flowing when $\tilde{\sigma}_0 \geq \frac{1}{\epsilon}B$ or, similarly, since $\tilde{\xi}_3 \leq 1+\tilde{\eta}$, when

$$\tilde{\xi}_3 \leq \tilde{Z}(\tilde{\xi}_1,\tilde{\xi}_2) = 1 + \tilde{\eta}(\tilde{\xi}_1,\tilde{\xi}_2) - \frac{B}{||\nabla_{\tilde{\xi}}\tilde{p}_L(\tilde{\xi}_1,\tilde{\xi}_2)||}$$

$\tilde{Z}(\tilde{\xi}_1,\tilde{\xi}_2)$ is the first order yield surface.

Finally, the terms in ϵ^0 of the velocity when $\tilde{\xi}_3 \leq \tilde{Z}(\tilde{\xi}_1,\tilde{\xi}_2) = 1+\tilde{\eta} - \frac{B}{||\nabla_{\tilde{\xi}}\tilde{p}_L||}$ are

$$\begin{aligned}\tilde{u}_0^1 &= \frac{1}{2}\tilde{\partial}\tilde{p}_{L1}\ \tilde{\xi}_3\left(\tilde{\xi}_3 - 2\left(1+\tilde{\eta} - \frac{B}{||\nabla_{\tilde{\xi}}\tilde{p}_L||}\right)\right)\\ \tilde{u}_0^2 &= \frac{1}{2}\tilde{\partial}\tilde{p}_{L2}\ \tilde{\xi}_3\left(\tilde{\xi}_3 - 2\left(1+\tilde{\eta} - \frac{B}{||\nabla_{\tilde{\xi}}\tilde{p}_L||}\right)\right)\end{aligned} \tag{B16}$$

11. Dimensional fluid dynamics of the Bingham layer

We recall that the local coordinate system is $(\mathbf{b}_1,\mathbf{b}_2,\mathbf{b}_3)$ and that the metric tensor is $C = (\mathbf{b}_i.\mathbf{b}_j)_{ij} = (g_{ij})_{ij}$ with its inverse being $C^{-1} = (g^{ij})_{ij}$.

As for the dimensionless case, we define for $i = 1,2$ the operator ∂q_i of a quantity q as

$$\partial q_i = g^{i1}\frac{\partial q}{\partial \xi_1} + g^{i2}\frac{\partial q}{\partial \xi_2} \tag{B17}$$

Then, we define the operator $\nabla_\xi\, q$ of a quantity q as

$$\nabla_\xi\, q = \partial q_1 \mathbf{b}_1 + \partial q_2 \mathbf{b}_2 \tag{B18}$$

and

$$\|\nabla_\xi\, q\| = \sqrt{\nabla_\xi\, q\,.\,\nabla_\xi\, q} = \sqrt{g_{11}(\partial q_1)^2 + g_{11}(\partial q_2)^2 + 2g_{12}\partial q_1 \partial q_2} \tag{B19}$$

Using these definitions, the dimensional stress is

$$\sigma(\xi_1,\xi_2,\xi_3) = (\tau+\eta-\xi_3)\ ||\nabla_\xi\, p_L|| + O(\epsilon)$$

The yield surface is located at

$$Z(\xi_1,\xi_2) = \tau + \eta - \frac{\sigma_y}{||\nabla_\xi\, p_L||} \tag{B20}$$

In the yielded region, i.e. where $\xi_3 \leq Z(\xi_1,\xi_2)$, the velocity at height ξ_3 is given by

$$\begin{cases} u^1(\xi_1,\xi_2,\xi_3,t) = -\dfrac{1}{2\mu}\partial p_{L1}\ \xi_3\left(2Z(\xi_1,\xi_2)-\xi_3\right) + O\left(U\epsilon\right) \\ u^2(\xi_1,\xi_2,\xi_3,t) = -\dfrac{1}{2\mu}\partial p_{L2}\ \xi_3\left(2Z(\xi_1,\xi_2)-\xi_3\right) + O\left(U\epsilon\right) \\ u^3(\xi_1,\xi_2,\xi_3,t) = O(U\epsilon) \end{cases} \tag{B21}$$

These results indicate that the normal velocity of the Bingham fluid layer, represented by $\frac{dX_{\mathcal{L}}}{dt} = u^3(\xi_1,\xi_2,\xi_3,t)\mathbf{b}_3$ (equation B2), is small relatively to the transversal velocities.

Moreover, we can exhibit a criterion on the curvature of the air–fluid interface indicating that the fluid is able to flow. This condition corresponds to $Z(\xi_1,\xi_2) > 0$, or, knowing that $p_L(\xi_1,\xi_2) = -2\gamma\kappa(\xi_1,\xi_2)$,

$$\|\nabla_\xi\,\kappa(\xi_1,\xi_2)\| < \frac{\sigma_y}{2\gamma(\tau+\eta(\xi_1,\xi_2))} \tag{B22}$$

Finally, the dominant velocity averaged over the thickness of the layer expresses in the frame (ξ_1,ξ_2,ξ_3):

$$\begin{cases} u^1_m(\xi_1,\xi_2,t) = -\frac{1}{2\mu}\partial p_{L1}\hat{Z}^2(\xi_1,\xi_2)\left(1-\frac{\hat{Z}(\xi_1,\xi_2)}{3(\tau+\eta)}\right) + O(U\epsilon) \\ u^2_m(\xi_1,\xi_2,t) = -\frac{1}{2\mu}\partial p_{L2}\hat{Z}^2(\xi_1,\xi_2)\left(1-\frac{\hat{Z}(\xi_1,\xi_2)}{3(\tau+\eta)}\right) + O(U\epsilon) \\ u^3_m(\xi_1,\xi_2,t) = O(U\epsilon) \\ \hat{Z}(\xi_1,\xi_2,t) = \max\left(0, \tau+\eta(\xi_1,\xi_2) - \frac{\sigma_y}{||\nabla_\xi\, p_L(\xi_1,\xi_2)||}\right) \end{cases}$$

or

$$\mathbf{u}_m(\xi_1,\xi_2,t) = -\frac{1}{2\mu}\hat{Z}^2(\xi_1,\xi_2)\left(1-\frac{\hat{Z}(\xi_1,\xi_2)}{3(\tau+\eta)}\right)\nabla_\xi\, p_L + O(U\epsilon) \tag{B23}$$

In order to compute the integrals on the ξ_3 direction, we used the property that if the fluid is yielded at the height ξ_3, it is yielded at all the heights smaller than ξ_3 since the stress is decreasing with ξ_3. For ξ_3 larger than $Z(\xi_1,\xi_2)$, the layer is solid and its velocity is the same as the velocity at the point $(\xi_1,\xi_2,\hat{Z}(\xi_1,\xi_2))$.

In the main text, we use the quantity $\theta(\xi_1,\xi_2) = \tau+\eta-\hat{Z}(\xi_1,\xi_2)$.

Appendix C: Velocity of the Bingham fluid layer averaged over a bifurcation in generation i

We assume now that $\eta = 0$. We consider now the wall of a bifurcation B_i in the generation i, parameterized by $X = f^i(u,v)$ with $(u,v) \in \Omega_i$. We denote $(\xi^i_1,\xi^i_2,\xi^i_3)$ the local coordinates system in B_i as defined in the Appendix B 1. Due to the structure of our model, we know that $(\xi^i_1,\xi^i_2,\xi^i_3) = h^i \times (\xi^0_1,\xi^0_2,\xi^0_3)$. The direction of the mucocilliary clearance is represented by the unit vector $\mathbf{t_m}(\xi^i_1,\xi^i_2)$, see Appendix E. By definition, the component of $\mathbf{t_m}$ along ξ_3 is 0. We define the variation of a quantity q in the direction of the mucocilliary clearance with

$$\frac{\partial_\xi q}{\partial m} = \nabla_\xi\, q(\xi^i_1,\xi^i_2)\ .\ \mathbf{t_m}(\xi^i_1,\xi^i_2)$$

The Bingham layer velocity in the direction of the mucociliary clearance averaged on the whole bifurcation B_i is

$$V_{m,i}\ = v_{\text{cilia}} - \tfrac{1}{|B_i|}\tfrac{1}{2\mu}\int_{B_i\cap\{(\xi^i_1,\xi^i_2)|Z_i(\xi^i_1,\xi^i_2)>0\}} \tfrac{\partial_\xi p_L}{\partial m}(\xi^i_1,\xi^i_2)\ Z^2_i(\xi^i_1,\xi^i_2)\left(1-\tfrac{Z_i(\xi^i_1,\xi^i_2)}{3\tau}\right)\|\tfrac{\partial f^i}{\partial u}\wedge\tfrac{\partial f^i}{\partial v}\|d\xi^i_1 d\xi^i_2$$

The condition $Z_i(\xi^i_1,\xi^i_2) > 0$ can be reformulated in $(\xi^0_1,\xi^0_2,\xi^0_3)$ using $Z_0(\xi^0_1,\xi^0_2)$ and i. It becomes $Z_0(\xi^0_1,\xi^0_2) > \tau\left(1-\frac{1}{h^{2i}}\right)$. Moreover $Z_i(\xi^i_1,\xi^i_2) = \tau - h^{2i}(\tau - Z_0(\xi^0_1,\xi^0_2))$. Recalling that $\nabla_\xi\, p_{L,i}(\xi^i_1,\xi^i_2) = -2\gamma\nabla_\xi\,\kappa_i(\xi^i_1,\xi^i_2) =$

$-\frac{2\gamma}{h^{2i}}\nabla_\xi\,\kappa_0(\xi_1^0,\xi_2^0)$, we can then express the previous equation using powers of $\left(\frac{\sigma_y h^{2i}}{2\tau\gamma}\frac{1}{||\nabla_\xi\,\kappa_0(\xi_1^0,\xi_2^0)||}\right)$,

$$\begin{aligned}
V_{m,i} = \; & v_{\text{cilia}} \\
& + \frac{1}{h^{2i}}\frac{2\gamma\tau^2}{3\mu|B_0|}\int_{B_0\cap\{(\xi_1^0,\xi_2^0)\;|\;||\nabla_\xi\,\kappa_0(\xi_1^0,\xi_2^0)||>\frac{\sigma_y}{2\tau\gamma}h^{2i}\}} \frac{\partial_\xi\kappa_0}{\partial m}(\xi_1^0,\xi_2^0)\left(\frac{\sigma_y h^{2i}}{2\tau\gamma}\frac{1}{||\nabla_\xi\,\kappa_0(\xi_1^0,\xi_2^0)||}\right)^0 \|\frac{\partial f^0}{\partial u}\wedge\frac{\partial f^0}{\partial v}\|d\xi_1^0 d\xi_2^0 \\
& - \frac{1}{h^{2i}}\frac{\gamma\tau^2}{\mu|B_0|}\int_{B_0\cap\{(\xi_1^0,\xi_2^0)\;|\;||\nabla_\xi\,\kappa_0(\xi_1^0,\xi_2^0)||>\frac{\sigma_y}{2\tau\gamma}h^{2i}\}} \frac{\partial_\xi\kappa_0}{\partial m}(\xi_1^0,\xi_2^0)\left(\frac{\sigma_y h^{2i}}{2\tau\gamma}\frac{1}{||\nabla_\xi\,\kappa_0(\xi_1^0,\xi_2^0)||}\right)^1 \|\frac{\partial f^0}{\partial u}\wedge\frac{\partial f^0}{\partial v}\|d\xi_1^0 d\xi_2^0 \\
& + \frac{1}{h^{2i}}\frac{\gamma\tau^2}{3\mu|B_0|}\int_{B_0\cap\{(\xi_1^0,\xi_2^0)\;|\;||\nabla_\xi\,\kappa_0(\xi_1^0,\xi_2^0)||>\frac{\sigma_y}{2\tau\gamma}h^{2i}\}} \frac{\partial_\xi\kappa_0}{\partial m}(\xi_1^0,\xi_2^0)(\left(\frac{\sigma_y h^{2i}}{2\tau\gamma}\frac{1}{||\nabla_\xi\,\kappa_0(\xi_1^0,\xi_2^0)||}\right)^3 \|\frac{\partial f^0}{\partial u}\wedge\frac{\partial f^0}{\partial v}\|d\xi_1^0 d\xi_2^0
\end{aligned} \tag{C1}$$

$$\begin{aligned}
V_{m,i} = \; & v_{\text{cilia}} + \frac{1}{h^{2i}}\frac{2\gamma\tau^2}{3\mu|B_0|}\int_{B_0\cap\{(\xi_1^0,\xi_2^0)\;|\;X_i(\xi_1^0,\xi_2^0)<1\}} \frac{\partial_\xi\kappa_0}{\partial m}(\xi_1^0,\xi_2^0)\times \\
& \left(1-\tfrac{3}{2}X_i(\xi_1^0,\xi_2^0)+\tfrac{1}{2}X_i(\xi_1^0,\xi_2^0)^3\right) \|\frac{\partial f^0}{\partial u}\wedge\frac{\partial f^0}{\partial v}\|d\xi_i^0 d\xi_2^0
\end{aligned}$$

with $X_i(\xi_1^0,\xi_2^0)=\frac{\sigma_y}{2\tau\gamma}\frac{h^{2i}}{||\nabla_\xi\,\kappa_0(\xi_1^0,\xi_2^0)||}$. If X_i is close to 1, then $1-\frac{3}{2}X_i(\xi_1^0,\xi_2^0)+\frac{1}{2}X_i(\xi_1^0,\xi_2^0)^3$ is small and the relative contribution to the whole integral is small. On the contrary, if X_i is small, then the relative contribution to the integral is maximal. Consequently, the integral is dominated by the contribution of the regions where X_i is small, i.e. where the curvature gradient is large.

Appendix D: Numerical simulations of the motion of a layer of a Bingham fluid on the wall of an airway tree

1. Geometry

The geometry of the three generations airway tree is based on typical sizes ratio measured in the lung [23]. The root branch diameter is 1 mm and the branch size decreases at each bifurcation with the ratio $\left(\frac{1}{2}\right)^{\frac{1}{3}}$. The ratio of length over diameter is 3. Two successive branching planes are rotating of 90 degrees from each other. The CAD geometry for GMSH is automatically built using Octave, STL surface meshes are generated using GMSH [36]. Visual details are given in Fig. 7.

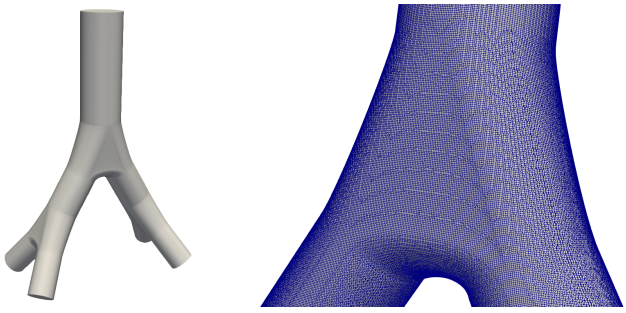

FIG. 5. The geometry and its surface mesh used in the simulations.

The curvature is computed from the surface divergence $k_0=\text{div}_S(\mathbf{n})$ of the inwards normals using boundary finite elements.

Actually, a (reasonably) crude mesh brings a good characterization of the main features of a bifurcation but will affect the quality of the variables computed with the finite elements method. On the contrary, a fine mesh brings high quality estimations with the finite elements method but brings noise on the curvature that is not meaningful to our approach. Hence, we smooth the curvature in order to allow the use of a mesh fine enough for the finite elements method while accounting for the main geometrical features of the bifurcation, independent on the mesh specificities. The curvature is smoothed using a technique from image analysis based on the heat equation [37]. The method is based on applying the heat equation on the divergence $k_0=\text{div}_S(\mathbf{n})$, that is considered as the initial state,

$$\begin{cases} \dfrac{\partial k}{\partial e}(\xi,e) - D\,\triangle_S\,k(\xi,e)=0 \text{ for } (\xi,e)\in\Omega\times]0,1] \\ k(\xi,0)=k_0(\xi) \end{cases}$$

Then the curvature used in our work is the field k taken at the time $e = 1$, i.e. $\kappa = k(., 1)$. The resulting smooth of the curvature corresponds to a convolution of the initial curvature field with a bi-dimensional Gaussian kernel

$$K(\xi) = \frac{1}{2\pi\sigma_{\mathrm{d}}^2} e^{-\frac{|\xi|^2}{2\sigma_{\mathrm{d}}^2}}$$

with a standard deviation $\sigma_{\mathrm{d}} = \sqrt{2D}$.

Then, we tested how the smoothing affects the mean Bingham fluid velocity in the bifurcation as a function of the mesh refinement, see Fig. 6. The degree of smoothing was then determined by the value for which the velocity was the closest for all the meshes tested, indicating that the result does not depend on the mesh size. The mesh size was fixed to 0.05 mm and the standard deviation of the smoothing to $\sigma_{\mathrm{d}} = 0.2$ mm, which corresponds to a diffusive coefficient $D = 2\ 10^{-8}\ \mathrm{m}^2.\mathrm{s}^{-1}$. The resulting smoothed curvature field is then used as the input of the computations of the model, see an example on Fig. **??**A.

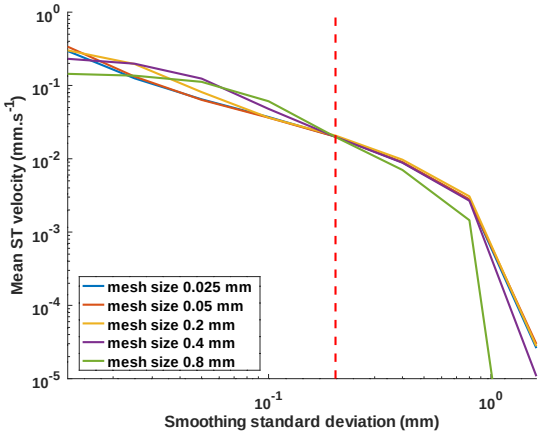

FIG. 6. Sensitivity of the mean Bingham fluid velocity (log-log) in the bifurcation relatively to the curvature smoothing (x-axis) and the mesh refinement (colored curves). The finer the mesh, the more precise is the quality of the finite elements method, but the more sensitive is the curvature to the mesh. If the smoothing standard deviation is too small, then the fluid velocity is affected by the mesh specificities, if it is too large, then the features of the bifurcation are lost. The degree of smoothing chosen is $\sigma_{\mathrm{d}} = 0.2$ mm. A smaller value induces artefacts due to the discretization in triangles of the bifurcation surface, while a larger value induces artefacts due to an over-smoothing that hide the main geometrical features of the bifurcation. The mesh size chosen was 0.05 mm with 186 594 triangles.

2. Numerical simulations

To study the properties of a thin layer of Bingham fluid in a 3D geometry, we used boundary finite elements within Comsol Multiphysics 3.5a.

The layer thickness has been based on the most frequent mean value reported in the literature for a healthy state, $\tau = 10\ \mu$m [15] and several values have been simulated up to 150 μm to mimic pathological thicknesses.

We estimated the characteristic size of the domain R using the airways radii. The thickness can be considered small relatively to the curvature radius in most of the generations of the tree. We indicated in the results when this hypothesis breaks. We use the results from lubrication theory of a Bingham fluid from Appendix B to estimate the main component of the thin Bingham fluid layer velocity.

Embedded capability of Comsol Multiphysics 3.5a are used to compute the tangential and normal vectors of a surface. Moreover, these vectors define an orthonormal local basis, allowing to get metric tensors $g^{(i,j)}$ and $g_{(i,j)}$ equal to the identity matrix. As a consequence, the dominant velocities of the Bingham layer averaged over its thickness

express as

$$\begin{cases} u_m^1(\xi_1,\xi_2) = -\frac{1}{2\mu}\frac{\partial p_L}{\partial \xi_1}\hat{Z}^2(\xi_1,\xi_2)\left(1-\frac{\hat{Z}(\xi_1,\xi_2)}{3(\tau+\eta)}\right)+O(U\epsilon) \\ u_m^2(\xi_1,\xi_2) = -\frac{1}{2\mu}\frac{\partial p_L}{\partial \xi_2}\hat{Z}^2(\xi_1,\xi_2)\left(1-\frac{\hat{Z}(\xi_1,\xi_2)}{3(\tau+\eta)}\right)+O(U\epsilon) \\ u_m^3(\xi_1,\xi_2) = O(U\epsilon) \\ \hat{Z}(x,y) = \max\left(0, \tau+\eta(\xi_1,\xi_2) - \frac{\sigma_y}{||\nabla_\xi p_L(\xi_1,\xi_2)||}\right) \end{cases}$$

We compute the mean curvature κ of the surface of the airway walls using the embedded surface derivatives in Comsol Multiphysics and computing the surface divergence of the normal $\mathbf{n}$ to the surface, i.e. $\kappa = \frac{1}{2}\mathrm{div}_s(\mathbf{n})$. To avoid a noisy curvature due to the meshing of the surface, the resulting curvature is smoothed locally using a kernel whose width is that of the mesh characteristic size.

The Laplace pressure is then computed as $p_L = -2\gamma\kappa$, with γ the surface tension, div_s the surface divergence and $\mathbf{n}$ the normal vector to the air–layer interface, oriented towards the bronchus interior where the air pressure is assumed to be 0.

Finally, we use again the surface derivatives to compute the derivatives of p_L, $\frac{\partial p_L}{\partial \xi_1}$ and $\frac{\partial p_L}{\partial \xi_1}$ along the two tangent directions to the airway walls.

Appendix E: Estimating the orientation of cilia velocity

Mucociliary motion of mucus was mimicked using a wall velocity of amplitude $v_{\text{cilia}} = 50\ \mu m.s^{-1}$. Directions of mucocilliary motion were determined by the directions of the gradient of a Laplacian L field whose source ($L = 1$) is at the inlet of the tree and well ($L = 0$) at the exits of the tree. No L flow was allowed through the wall of the tree. The wall gradient of such a field is smooth, tangent to the wall and parallel to the centerlines of the tree. We assumed that the velocity induced on mucus by mucocilliary transport is

$$\mathbf{v}_{\text{cilia}} = v_{\text{cilia}} \times \frac{\nabla L}{||\nabla L||}$$

Another way for estimating the velocity wall field was chosen in [20]. However the properties of the field obtained by

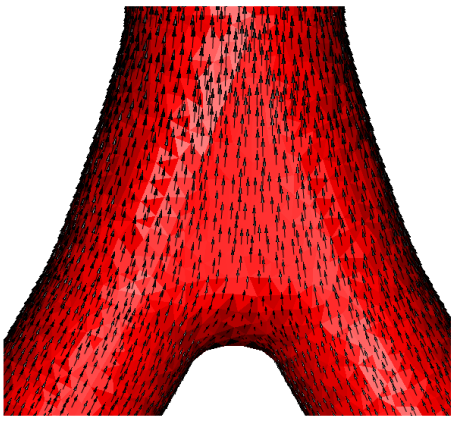

FIG. 7. Details of a bifurcation to show the direction of the motion of mucus due to cilia predicted by our model based on the gradient of a Laplacian field.

our method and the properties of the field obtained in [20] are very close. The method proposed here allows to compute a velocity wall field without computing the centerlines of the tree, which can be useful for complex geometries.

As discussed in [15], the assumption of a constant velocity of the mucus layer whatever the depth in the bronchial tree brings is not compatible with a constant mucus layer thickness throughout the tree. Indeed, flow conservation in bifurcation consisting in a branch with radius r_i that bifurcates into two branches with radii $r_{i+1} = hr_i$, allows to relate the respective mucus layer thicknesses τ_i and τ_{i+1}

$$\underbrace{2\pi r_i\ \tau_i\ v_{\text{cilia}}}_{\text{outflow of branch } i} = \underbrace{2\times 2\pi r_{i+1}\ \tau_{i+1}\ v_{\text{cilia}}}_{\text{outflow of branches } i+1} \longrightarrow\ \tau_i = 2h\ \tau_{i+1} \simeq 1.59\ \tau_{i+1}$$

Hence the observed relative homogeneous thickness of the mucus layer in the bronchi might be the results of a regulation by other mechanisms [15]. The way we mimicked mucociliary clearance in this study does not account for these potential other regulation mechanisms and does not allow for a conservation of the layer thickness.